Chapter 3

Design and Analysis of Integrated Cross-grid Array Routing Wavelength Switch by Microring Resonator Based on SOI Waveguide

As mentioned in Chapter 2, the integrated development of optical waveguide devices has become the future trend. We propose optical waveguide components for DWDM device and Optical Switch building on SOI wafers by microring in this chapter. Based on our design parameters as chapter 2 mentioned, we will use those parameters of this microring to simulate and analyze the expand structure such as 4×4、8×8、16×16 and 32×32 optical wavelength routing switch. With different input and output channel number the insertion loss and the switching voltage need will different. This chapter is organized as follows: Section 3-1 introduces the advance structure of optic-electronic integrated circuits to form the access network. The advantages of SOI microring resonator applied in integrated optics are presented and discussed. In the section 3-2, I will show the mathematical formulation of N×N cascade transmission scattering matrix approach. The simulation results of 4×4 port microring resonator routing wavelength switch structure are discussed in Section 3-3-1. The simulation results of 8×8 port microring resonator routing wavelength switch structure are discussed in Section 3-3-2. The simulation results of 16×16 port microring resonator routing wavelength switch structure are discussed in Section 3-3-3.The simulation results of our designed 32×32 port microring resonator access network structure are also discussed in Section 3-3-4. Besides, the characteristics of our designed 32×32 microring routing are also presented in Section 3-4. Then we give the conclusions and discussions of our designed microring routing wavelength switch devices in the final Section 3-5.

3-1 Introduction of A Cross-grid Array Optical Routing Wavelength Switch by Microring Resonators Structure

In the near future, large scale integrated optical systems with densely packed simple optical components will constitute the building blocks of optical communications networks and signal processing circuits. These optical circuits are faster, more scalable, and potentially less expensive than their hybrid optical analogs. Precise modeling and exacting fabrication of dielectric structures are necessary to build the next generation of integrated optical systems. Also essential are new techniques for accurate characterization of such optical systems, from the most basic building blocks like simple channel waveguides to novel structures such as micro-ring resonators for wavelength division multiplexing. Microring resonators serve as robust, ultra-compact devices for optical communications [105–109]. Included among their many applications are add–drop filters for dense-wavelength-division-multiplexed (DWDM) networks. For instance, 1×8 add–drop filters using 10μm radius rings have been demonstrated [110]. Because of their compact size, device integration densities of upward of 10^5 devices/cm^2 can be envisioned. Complex circuits involving several resonators per node for improved performance can be employed without concern for chip space. In this chapter, we discuss and demonstrate the use of designed resonators for the purpose of multiple cascade microrings to be the optical access network. A cross-grid array [111] microring resonator above high refractive index contrast silicon/sio_2 waveguides was introduced as a scalable architecture for building complex optical circuits. The waveguides are laid out on a grid pattern, and cross through each other at points of intersection.

3-2 Mathematical Formulation of Cross-grid Array Transmission Scattering Matrix Approach by Microring Resonator

A scalable architecture for accessing the entire surface of a chip with high integration density is depicted schematically in Fig. 3-1. Fig. 3-1 shows the physical implementation while the functional block diagram of the array. We call this architecture the cross-grid array. It is comprised of channel waveguides crossing through each other in a Manhattan-like grid pattern. A ring or multiple ring resonator devices is side coupled to, or vertically integrated above, each crossing junction. The rings serve as wavelength selective cross-connects. The region consisting of a junction and a ring cross-connect is called a cross-grid node as Fig. 3-2 shows. In this transformation, we will be able to apply a transmission matrix approach. The details of wave propagation within a single node are depicted in Fig. 3-2. The labeling consists of wave amplitude A with a superscript "＋" or "－"means a in to the node or outgoing from the node traveling wave respectively, subscript "U"、"D"、"L" or "R" designating the upper ward、 Downward、Left or Right waveguides of the four port node transition direction respectively. The scattering matrix of the four-port node consists of the response of the ring device combined with the effects of scattering at the waveguide crossing junction. Waveguide scattering at a junction is also depicted. The quantity “s” is the fractional amplitude scattered into the orthogonal ports. The scattering matrix for the four port which depicted in Fig. 3-2 has the form:

$$A_{out} = S_i \cdot A_{in} \tag{3-1}$$

Where S_i is the 4×4 scattering matrix for node *i*, $A_{in} = \left[A_U^+, A_L^+, A_D^-, A_R^-\right]^T$ is the input wave amplitudes incident on the node, and $A_{out} = \left[A_U^-, A_L^-, A_D^+, A_R^+\right]^T$ is the scattered wave amplitude. The elements of S_i, correct to first order in the scattering parameters s are:

$$s_{11} = s_{44} = j2s\tau \operatorname{Re}^{\left(-j2\phi_c - j\phi\right)} \tag{3-2}$$

$$s_{21} = s_{43} = j2sFe^{c\left(-j\phi_g\right)}, \quad s_{22} = s_{33} = 0 \tag{3-3}$$

$$s_{41} = s_{32} = \tau F\left(1 + js\operatorname{Re}^{\left(-j2\phi_c\right)}\right)e^{\left(-j\phi\right)} \tag{3-4}$$

$$s_{31} = \left(\gamma^2 \operatorname{Re}^{\left(-j2\phi_c\right) + js\left(1 + (\tau R)^2 e\left(-j4\phi_c\right)\right)}\right) \times e^{-j\phi_{gc}} \tag{3-5}$$

$$s_{42} = \left(\operatorname{Re}^{\left(j2\phi\right)} + jsF^2\right)e^{\left(-j\phi_g\right)} \tag{3-6}$$

where ϕ_c is the optical phase delay between the junction position and the coupling position for the ring, and ϕ_g is the phase delay between any two junctions, assuming all junctions are equidistant. *R* is the ring resonator device filter response at the drop port (i.e., A_L^+ and A_D^+ in the absence of the junction), while is the straight through response (i.e., A_L^+ and A_R^- in the absence of the junction.) All scattering elements are with reference to the center of the crossing junction. The remaining elements can be found from the symmetry requirement $S_{ij} = S_{ji}$. Analytic expressions are available for and in [111] and [112]. The N×N The array in Fig. 3-1 is subdivided into 2N parts as shown by the dashed lines. Each section is described by a (4N)×(4N) transmission matrix M_i, which propagates all the waves on the left side of a section to those on the right side. The matrices M_i are easily constructed, with the elements consisting of: (1). the relevant 4×4 transmission matrices T_j of each node *j*th in the *i*th section, centered on the appropriate part of the diagonal of M_i. (2). diagonal elements equal to unity where there are straight through connections and (3). Zeros everywhere else. The overall transmission matrix M is a cascade product of the sections.

$$M = M_1 \cdot M_2 \cdots M_{2N-2} \cdot M_{2N-1} \tag{3-7}$$

The scattering matrix for the entire array is found by transforming matrix **M** by well known methods [113].

3-3 Design and Analysis of Cross-grid Array optical Wavelength Switch by SOI Microring Resonator

In this section, we design an N×N microring resonator (MRR) routing switch based on free carrier plasma effect to build the active control network. Modeling and simulation results on novel resonant cascade microring resonator such as 4×4 switches、8×8 switches、16×16 switches and 32×32 switches to be optical cross connect network are presented here. Those advantages of employed N×N cascade microring routing wavelength switch will be analyzed and discussed. For the designed N×N optical cross connect network, the routing path from arbitrary input port to arbitrary output port could be modulated only by two control elements (ring resonator). Electro-optic switching at used ITU wavelength is investigated and the wavelength spacing is 0.4 nm. A novel peaks-and-valley spectral response allows low-power switching with low crosstalk and least control elements. Complete switching is attained when the effect refractive index of both rings is perturbed by $\Delta n = 3.1\times10^{-2} \sim 2\times10^{-3}$. This chapter presents new designs and simulations for resonant, electro-optic 4×4、8×8、16×16 and 32×32 routing wavelength switches. Each in plane device contains identical side coupling microring at the same plane

Many N×N interconnection geometries are thereby feasible. Generally, these active resonant devices are part of the emerging trend of microphotonic integration upon silicon, where in the interconnected waveguide components comprise a highly functional chip-scale optical network amenable to optoelectronic integration upon CMOS. Advances in microring device design will allow the ring diameter to be reduced, in some cases, from 50 micros to just a few micros, thus enabling a higher packing density of components and promoting. Simulation of the drop-port and through-port outputs is based in this paper upon our use in chapter 2 to analyze the filter response of high-Q ring devices in the OFF and ON states, where OFF can refer to a particular index bias point.

3-3-1 Design and Analysis of 4×4 Optical Routing Wavelength Switching by SOI Microring Resonator

In this section, we design an 4×4 microring cross grid wavelength switching network based on free carrier plasma effect by FDTD method.

We simulate the routing effect from arbitrary input port to any other output port by controlling the individual ring waveguide refractive index. The optical wavelength switch with adding various voltages on several electrode pad regions to control light signal switching path are also simulated. The size of the 4×4 wavelength switching network is 75μm×30μm. Fig. 3-3 shows the top view of our designed 4×4 optical wavelength switching network with 8 microrings as control elements. With tuning the voltages on several electrode pads and use the different change of refractive index on several regions to control the light wave propagation path. We use the ITU 0.4nm wavelength spacing to launch into the microring optical wavelength switch. Those wavelengths are 1540nm, 1540.4nm, 1540.8 nm and 1541.2nm. In addition to all of the above, we can switch the light wave propagate from one of 4 input port channels to one of 4 output port channels as aspiration. Fig. 3-4 shows a light wavelength 1540nm launching into input port 1 at our designed 4×4 optical wavelength switching network. Fig. 3-4(a) shows a light wavelength 1540nm propagate from input 1 to output 1 and the transmittance value of the output4 is –1.199dBm. With didn't add any voltages on several electrode pads, the light transmit straightly to the output4. Fig. 3-4(b) shows a light wavelength 1540nm propagate from input1 to output2 and the transmittance value of the output2 is –3.782 dBm. We add voltages on several electrode pads such as R_1 and R_2 and use the change of refractive index ($\triangle n = -2.4\times10^{-2}$) on several regions to control the light wave propagation path. Fig. 3-4(c) shows a light wavelength 1540nm propagate from input1 to output3 and the transmittance value of the output3 is –4.678dBm. We add voltages on several fingered electrode pads such as R_1 and R_3 and use the change of refractive index ($\triangle n = -2.4\times10^{-2}$) on several regions to control the light wave propagation path. Fig. 3-4(d) shows a light wavelength 1540nm propagate from input1 to output4 and the transmittance value of the output16 is –5.269dBm. We add voltages on several fingered electrode pads such as R_1 and R_4 and use the change of refractive index (△n=–2.4×10^{-2}) on several regions to control the light wave propagation path.

Fig. 3-5 shows a light wavelength 1540nm launching into input port 2 at our designed 4×4 optical wavelength switching network. Fig. 3-5(a) shows a light wavelength 1540nm propagate from input2 to output1 and the transmittance value of the output4 is –4.636dBm. We add voltages on several electrode pads such as R_6 and R_5 and use the change of refractive index (△n=–2.4×10^{-2}) on several regions to control the light wave propagation path. Fig. 3-5(b) shows a light wavelength 1540nm propagate from input2 to output2 and the transmittance value of the output8 is –1.432dBm. With didn't add any voltages on several electrode pads, the light transmit straightly to the output2. Fig. 3-5(c) shows a light wavelength 1540nm propagate from input2 to output3 and the transmittance value of the output3 is –4.778dBm. We add voltages on several fingered electrode pads such as R_2 and R_3 and use the change of refractive index (△n=–2.4×10^{-2}) on several regions to control the light wave propagation path. Fig. 3-5(d) shows a light wavelength 1540nm propagate from input2 to output4 and the transmittance value of the output4 is –5.569dBm. We add voltages on several fingered electrode pads such as R_2 and R_4 and use the change of refractive index (△n=–2.4×10^{-2}) on several regions to control the light wave propagation path.

Fig. 3-6 shows a light wavelength 1540nm launching into input port 3 at our designed 4×4 optical wavelength switching network. Fig. 3-6(a) shows a light wavelength 1540nm propagate from input3 to output1 and the transmittance value of the output4 is –4.853dBm. We add voltages on several electrode pads such as R_7 and R_5 and use the change of refractive index ($\triangle n = -2.4 \times 10^{-2}$) on several regions to control the light wave propagation path. Fig. 3-6(b) shows a light wavelength 1540nm propagate from input3 to output2 and the transmittance value of the output2 is –4.182dBm. We add voltages on several fingered electrode pads such as R_7 and R_6 and use the change of refractive index ($\triangle n = -2.4 \times 10^{-2}$) on several regions to control the light wave propagation path. Fig. 3-6(c) shows a light wavelength 1540nm propagate from input3 to output3 and the transmittance value of the output3 is –1.278dBm. With didn't add any voltages on several electrode pads, the light transmit straightly to the output12. Fig. 3-6(d) shows a light wavelength 1540nm propagate from input3 to output4 and the transmittance value of the output4 is –4.216dBm. We add voltages on several fingered electrode pads such as R_3 and R_4 and use the change of refractive index ($\triangle n = -2.4 \times 10^{-2}$) on several regions to control the light wave propagation path.

Fig. 3-7 shows a light wavelength 1540nm launching into input port 4 at our designed 4×4 optical wavelength switching network. Fig. 3-7(a) shows a light wavelength 1540nm propagate from input4 to output1 and the transmittance value of the output1 is –6.053dBm. We add voltages on several electrode pads such as R_8 and R_5 and use the change of refractive index ($\triangle n = -2.4 \times 10^{-2}$) on several regions to control the light wave propagation path. Fig. 3-7(b) shows a light wavelength 1540nm propagate from input4 to output2 and the transmittance value of the output8 is –5.382dBm. We add voltages on several fingered electrode pads such as R_8 and R_6 and use the change of refractive index ($\triangle n = -2.4 \times 10^{-2}$) on several regions to control the light wave propagation path. Fig. 3-7(c) shows a light wavelength 1540nm propagate from input4 to output3 and the transmittance value of the output3 is –4.678dBm. We add voltages on several fingered electrode pads such as R_8 and R_7 and use the change of refractive index ($\triangle n = -2.4 \times 10^{-2}$) on several regions to control the light wave propagation path. Fig. 3-7(d) shows a light wavelength 1540nm propagate from input4 to output4 and the transmittance value of the output8 is –1.416dBm. With didn't add any voltages on several electrode pads, the light transmit straightly to the output4.

Fig. 3-8 shows an ITU light wavelength from 1540 nm to 1541.2 nm launching into each input port from channel1 to channel16 at our designed 4×4 microring routing wavelength switch individually. The total number of our input wavelength is 4 and the channel spacing is 0.4nm. In this case, we add voltages on several electrode pads and use the various change of refractive index from -2.144×10^{-2} to -2.4×10^{-2} on several regions to control the light wave propagation path. The regions of adding voltages and the change of refractive index on several electrode pads such as $R_1 = R_4 = -2.4 \times 10^{-2}$ for wavelength = 1540nm, $R_2 = R_3 = -2.341 \times 10^{-2}$ for wavelength = 1540.4nm, $R_6 = R_7 = -2.243 \times 10^{-2}$ for wavelength = 1540.8nm, $R_8 = R_5 = -2.144 \times 10^{-2}$.

Fig. 3-8(a) shows the simulation results of (1)-(4) for ITU wavelength from 1540nm to 1541.2nm launching into 4×4 microring routing wavelength switch from input port1 to input port4. Fig. 3-8(a) show a light wavelength 1540nm propagate from input1 to output4 and the transmittance value of the output4 is –5.269dBm. Fig. 3-8(b) show a light wavelength 1540.2nm propagate from input2 to output3 and the transmittance value of the output3 is –4.778dBm. Fig. 3-8(c) show a light wavelength 1540.8nm propagate from input3 to output12 and the transmittance value of the output2 is –4.582dBm. Fig. 3-8(d) show a light wavelength 1541.2nm propagate from input4 to output1 and the transmittance value of the output1 is –5.915dBm.

In addition to before we mentioned, we also simulate the other four wavelength individual launching into input port. Fig. 3-9 shows the output power at individual output channel with different refractive index change for the four wavelength individual launching into input port 1. Fig. 3-10 shows the output power at individual output channel with different refractive index change for the four wavelength individual launching into input port 2. Fig. 3-11 shows the output power at individual output channel with different refractive index change for the four wavelength individual launching into input port 3. Fig. 3-12 shows the output power at individual output channel with different refractive index change for the four wavelength individual launching into input port 4. Fig. 3-13 shows the output power at individual 4 output ports with different refractive index change for ITU wavelength launching into switch device

3-3-2 Design and Analysis of 8×8 Optical Routing Wavelength Switch by SOI Microring Resonator

In this section, we design an 8×8 microring cross grid wavelength switching network based on free carrier plasma effect by FDTD method. We simulate the routing effect from arbitrary input to any other out put by controlling the individual ring waveguide refractive index. The optical wavelength switch with adding various voltages on several electrode pad regions to control light signal switching path are also simulated. The size of the 8×8 wavelength switching network is 150μm×30μm. Fig. 3-14 shows the top view of our designed 8×8 optical wavelength switching network with 16 microrings as control elements. With tuning the voltages on several electrode pads and use the different change of refractive index on several regions to control the light wave propagation path. In addition to all of the above, we can switch the light wave propagate from one of 8 input channels to one of 8 output port channels as desire.

We use the ITU 0.4nm wavelength spacing to launch into the microring optical wavelength switch. In addition to all of the above, we can switch the light wave propagate from one of 8 input channels to one of 8 output channels as aspiration. Fig. 3-15 shows a light wavelength 1540nm launching into input port 2 at our designed 8×8 optical wavelength switching network. Fig. 3-15(a) shows a light wavelength 1540nm propagate from input 2 to output 2 and the transmittance value of the output2 is –1.266dBm. With didn't add any voltages on several electrode pads, the light transmit straightly to the output2. Fig. 3-15(b) shows a light wavelength 1540nm propagate from input2 to output4 and the transmittance value of the output4 is –4.769dBm. We add voltages on several electrode pads such as R_2 and R_4 and use the change of refractive index ($\triangle n = -2.4\times10^{-2}$)on several regions to control the light wave propagation path. Fig. 3-15(c) shows a light wavelength 1540nm propagate from input2 to output6 and the transmittance value of the output6 is –5.841dBm. We add voltages on several fingered electrode pads such as R_2 and R_6 and use the change of refractive index ($\triangle n = -2.4\times10^{-2}$) on several regions to control the light wave propagation path. Fig. 3-15(d) shows a light wavelength 1540nm propagate from input2 to output8 and the transmittance value of the output8 is –7.485dBm. We add voltages on several fingered electrode pads such as R_2 and R_8 and use the change of refractive index ($\triangle n = -2.4\times10^{-2}$) on several regions to control the light wave propagation path.

Fig. 3-16 shows a light wavelength 1540nm launching into input port

4 at our designed 8×8 optical wavelength switching network. Fig. 3-16(a) shows a light wavelength 1540nm propagate from input4 to output2 and the transmittance value of the output2 is –5.763dBm. We add voltages on several electrode pads such as R_{12} and R_{10} and use the change of refractive index (△n=–2.4×10^{-2}) on several regions to control the light wave propagation path. Fig. 3-16(b) shows a light wavelength 1540nm propagate from input4 to output4 and the transmittance value of the output4 is –1.457dBm. With didn't add any voltages on several electrode pads, the light transmit straightly to the output8. Fig. 3-16(c) shows a light wavelength 1540nm propagate from input4 to output6 and the transmittance value of the output6 is –5.394dBm. We add voltages on several fingered electrode pads such as R_4 *a*nd R_6 and use the change of refractive index (△n=–2.4×10^{-2}) on several regions to control the light wave propagation path. Fig. 3-16(d) shows a light wavelength 1540nm propagate from input4 to output8 and the transmittance value of the output8 is –6.752dBm. We add voltages on several fingered electrode pads such as R_4 and R_8 and use the change of refractive index (△n=–2.4×10^{-2}) on several regions to control the light wave propagation path.

Fig. 3-17 shows a light wavelength 1540nm launching into input port 6 at our designed 8×8 optical wavelength switching network. Fig. 3-17(a) shows a light wavelength 1540nm propagate from input6 to output2 and the transmittance value of the output2 is –6.166dBm. We add voltages on several electrode pads such as R_{14} and R_{10} and use the change of refractive index (△n=–2.4×10^{-2}) on several regions to control the light wave propagation path. Fig. 3-17(b) shows a light wavelength 1540nm propagate from input6 to output4 and the transmittance value of the output4 is –4.669dBm. We add voltages on several fingered electrode pads such as R_{14} and R_{12} and use the change of refractive index (△n=–2.4×10^{-2}) on several regions to control the light wave propagation path. Fig. 3-17(c) shows a light wavelength 1540nm propagate from input16 to output6 and the transmittance value of the output6 is –1.353dBm. With didn't add any voltages on several electrode pads, the light transmit straightly to the output12. Fig. 3-17(d) shows a light wavelength 1540nm propagate from input6 to output8 and the transmittance value of the output18 is –4.849dBm. We add voltages on several fingered electrode pads such as R_6 and R_8 and use the change of refractive index ($\triangle$n=–2.4×10^{-2}) on several regions to control the light wave propagation path.

Fig. 3-18 shows a light wavelength 1540nm launching into input port 8 at our designed 8×8 optical wavelength switching network. Fig. 3-18(a) shows a light wavelength 1540nm propagate from input8 to output2 and the transmittance value of the output2 is –8.324dBm. We add voltages on several electrode pads such as R_{16} and R_{10} and use the change of refractive index ($\triangle$n=–2.4×10^{-2}) on several regions to control the light wave propagation path. Fig. 3-18(b) shows a light wavelength 1540nm propagate from input8 to output4 and the transmittance value of the output4 is –6.843dBm. We add voltages on several fingered electrode pads such as R_{16} and R_{12} and use the change of refractive index ($\triangle$n=–2.4×10^{-2}) on several regions to control the light wave propagation path. Fig. 3-18(c) shows a light wavelength 1540nm propagate from input8 to output6 and the transmittance value of the output6 is –5.459dBm. We add voltages on several fingered electrode pads such as R_{16} and R_{14} and use the change of refractive index ($\triangle$n=–2.4×10^{-2}) on several regions to control the light wave propagation path. Fig. 3-18(d) shows a light wavelength 1540nm propagate from input8 to output8 and the transmittance value of the output8 is –1.152dBm. With didn't add any voltages on several electrode pads, the light transmit straightly to the output8.

Fig. 3-19 and Fig. 3-20 shows an ITU light wavelength from 1540nm to 1542.8nm launching into each input port from channel1 to channel8 at our designed 8×8 microring routing wavelength switch individually. The total number of our input wavelength is 8 and the channel spacing is 0.4nm. In this case, we add voltages on several electrode pads and use the various change of refractive index from -1.75×10^{-2} to -2.4×10^{-2} on several regions to control the light wave propagation path. The regions of adding voltages and the change of refractive index on several fingered electrode pads such as $R_1 = R_8 = -2.4\times10^{-2}$ for wavelength =1540nm, $R_2 = R_7 = -2.341\times10^{-2}$ for wavelength = 1540.4, $R_3 = R_6 = -2.243\times10^{-2}$ for wavelength = 1540.8nm, $R_4 = R_5 = -2.144\times10^{-2}$ for wavelength = 1541.2nm, $R_{13} = R_{12} = -2.04\times10^{-2}$ for wavelength = 1541.6nm, $R_{14} = R_{11} = -1.95\times10^{-2}$ for wavelength = 1542nm, $R_{15} = R_{10} = -1.85\times10^{-2}$ wavelength = 1542.4nm, $R_{16} = R_9 = -1.75\times10^{-2}$ wavelength = 1542.8nm.

Fig. 3-19 shows the simulation results of (a)-(d) for ITU wavelength from 1538.8nm to 1540nm launching into 8×8 microring routing wavelength switch from input port1 to input port4. Fig. 3-19(a) show a light wavelength 1538.8nm propagates from input1 to output8 and the transmittance value of the output8 is –7.912dBm. Fig. 3-19(b) show a light wavelength 1539.2nm propagate from input2 to output7 and the transmittance value of the output7 is –6.322dBm. Fig. 3-19(c) show a light wavelength 1539.6nm propagate from input3 to output6 and the transmittance value of the output6 is –5.137dBm. Fig. 3-19(d) show a light wavelength 1540nm propagate from input4 to output5 and the transmittance value of the output5 is –8.545dBm.

Fig. 3-20 shows the simulation results of (a)-(d) for ITU wavelength from 1540.4nm to 1541.6nm launching into 8×8 microring routing wavelength switch from input port5 to input port8. Fig. 3-20(a) show a light wavelength 1540.4nm propagate from input5 to output4 and the transmittance value of the output4 is –4.272dBm. Fig. 3-20(b) show a light wavelength 1540.8nm propagate from input6 to output3 and the transmittance value of the output3 is –5.378dBm. Fig. 3-20(c) show a light wavelength 1541.2nm propagate from input7 to output2 and the transmittance value of the output2 is –7.913dBm. Fig. 3-20(d) show a light wavelength 1541.6nm propagate from input8 to output1 and the transmittance value of the output1 is –9.149dBm.

In addition to before we mentioned, we also simulate the four wavelength individual launching into input port. Fig. 3-21 shows the output power at individual output channel with different refractive index change for the four wavelength individual launching into input port 2. Fig. 3-22 shows the output power at individual output channel with different refractive index change for the four wavelength individual launching into input port 4. Fig. 3-23 shows the output power at individual output channel with different refractive index change for the four wavelength individual launching into input port 6. Fig. 3-24 shows the output power at individual output channel with different refractive index change for the four wavelength individual launching into input port 8. Fig. 3-25 shows the output power at individual 4 output ports with different refractive index change for ITU wavelength launching into 8×8 grid array microring resonator wavelength switch device.

3-3-3 Design and Analysis of 16×16 Optical Routing Wavelength Switch by SOI Microring Resonator

In this section, we design an 16×16 microring cross grid wavelength switching network based on free carrier plasma effect by FDTD method. We simulate the routing effect from arbitrary input to any other out put by controlling the individual ring waveguide refractive index. The optical wavelength switch with adding various voltages on several electrode pad regions to control light signal switching path are also simulated. The size of the 16×16 wavelength switching network is 300μm×30μm. Fig. 3-26 shows the top view of our designed 16×16 optical wavelength switching network with 32 microrings as control elements. With tuning the voltages on several electrode pads and use the different change of refractive index on several regions to control the light wave propagation path. We use the ITU 0.4nm wavelength spacing to launch into the microring optical wavelength switch. In addition to all of the above, we can switch the light wave propagate from one of 16 input channels to one of 16 output channels as aspiration. Fig. 3-27 shows a light wavelength 1540nm launching into input port 4 at our designed 16×16 optical wavelength switching network. Fig. 3-27(a) shows a light wavelength 1540nm propagate from input 4 to output 4 and the transmittance value of the output4 is –1.199dBm. With didn't add any voltages on several electrode pads, the light transmit straightly to the output4. Fig. 3-27(b) shows a light wavelength 1540nm propagate from input4 to output8 and the transmittance value of the output8 is -6.234dBm. We add voltages on several electrode pads such as R_4 and R_8 and use the change of refractive index ($\triangle n = -2.4\times10^{-2}$)on several regions to control the light wave propagation path. Fig. 3-27(c) shows a light wavelength 1540nm propagate from input4 to output12 and the transmittance value of the output24 is –9.029dBm. We add voltages on several fingered electrode pads such as R_4 and R_{12} and use the change of refractive index (△n=–2.4×10^{-2}) on several regions to control the light wave propagation path. Fig. 3-27(d) shows a light wavelength 1540nm propagate from input4 to output16 and the transmittance value of the output16 is –12.752dBm. We add voltages on several fingered electrode pads such as R_4 and R_{16} and use the change of refractive index (△n=–2.4×10^{-2}) on several regions to control the light wave propagation path.

Fig. 3-28 shows a light wavelength 1540nm launching into input port 8 at our designed 16×16 optical wavelength switching network. Fig. 3-28(a) shows a light wavelength 1540nm propagate from input8 to output4 and the transmittance value of the output4 is –6.179dBm. We add voltages on several electrode pads such as R_{24} and R_{20} and use the change of refractive index (△n=–2.4×10^{-2}) on several regions to control the light wave propagation path. Fig. 3-28(b) shows a light wavelength 1540nm propagate from input8 to output8 and the transmittance value of the output8 is –1.127dBm. With didn't add any voltages on several electrode pads, the light transmit straightly to the output8. Fig. 3-28(c) shows a light wavelength 1540nm propagate from input8 to output12 and the transmittance value of the output24 is –6.172dBm. We add voltages on several fingered electrode pads such as R_8 and R_{12} and use the change of refractive index (△n=–2.4×10^{-2}) on several regions to control the light wave propagation path. Fig. 3-28(d) shows a light wavelength 1540nm propagate from input4 to output16 and the transmittance value of the output16 is –7.422dBm. We add voltages on several fingered electrode pads such as R_8 and R_{16} and use the change of refractive index (△n=–2.4×10^{-2}) on several regions to control the light wave propagation path.

Fig. 3-29 shows a light wavelength 1540nm launching into input port

12 at our designed 16×16 optical wavelength switching network. Fig. 3-29(a) shows a light wavelength 1540nm propagate from input12 to output4 and the transmittance value of the output4 is –8.653dBm. We add voltages on several electrode pads such as R_{28} and R_{20} and use the change of refractive index (△n=–2.4×10^{-2}) on several regions to control the light wave propagation path. Fig. 3-29(b) shows a light wavelength 1540nm propagate from input12 to output8 and the transmittance value of the output8 is –6.014dBm. We add voltages on several fingered electrode pads such as R_{28} and R_{24} and use the change of refractive index (△n=–2.4×10^{-2}) on several regions to control the light wave propagation path. Fig. 3-29(c) shows a light wavelength 1540nm propagate from input12 to output12 and the transmittance value of the output8 is –1.029dBm. With didn't add any voltages on several electrode pads, the light transmit straightly to the output12. Fig. 3-29(d) shows a light wavelength 1540nm propagate from input4 to output16 and the transmittance value of the output16 is –5.652dBm. We add voltages on several fingered electrode pads such as R_{12} and R_{16} and use the change of refractive index (△n=–2.4×10^{-2}) on several regions to control the light wave propagation path.

Fig. 3-30 shows a light wavelength 1540nm launching into input port 16 at our designed 16×16 optical wavelength switching network. Fig. 3-30(a) shows a light wavelength 1540nm propagate from input16 to output4 and the transmittance value of the output4 is –13.484dBm. We add voltages on several electrode pads such as R_{32} and R_{20} and use the change of refractive index (△n=–2.4×10^{-2}) on several regions to control the light wave propagation path. Fig. 3-30(b) shows a light wavelength 1540nm propagate from input16 to output8 and the transmittance value of the output8 is –8.534dBm. We add voltages on several fingered electrode pads such as R_{32} and R_{24} and use the change of refractive index (△n=–2.4×10^{-2})

on several regions to control the light wave propagation path. Fig. 3-30(c) shows a light wavelength 1540nm propagate from input16 to output12 and the transmittance value of the output12 is –5.652dBm. We add voltages on several fingered electrode pads such as R_{32} and R_{28} and use the change of refractive index ($\triangle$n=–2.4×10^{-2}) on several regions to control the light wave propagation path. Fig. 3-30(d) shows a light wavelength 1540nm propagate from input16 to output16 and the transmittance value of the output8 is –1.052dBm. With didn't add any voltages on several electrode pads, the light transmit straightly to the output16.

Fig. 3-31 to Fig. 3-34 shows an ITU light wavelength from 1538.8 nm to 1544.8nm launching into each input port from channel1 to channel16 at our designed 16×16 microring routing wavelength switch individually. The total number of our input wavelength is 16 and the channel spacing is 0.4nm. In this case, we add voltages on several electrode pads and use the various change of refractive index from –1.26×10^{-2} to –2.73×10^{-2} on several regions to control the light wave propagation path. The regions of adding voltages and the change of refractive index on several fingered electrode pads such as $R_1 = R_{16}$ = –2.73×10^{-2} for wavelength= 1538.8nm, $R_2 = R_{15}$ = –2.63×10^{-2} for wavelength= 1539.2nm, $R_3 = R_{14}$ = –2.53×10^{-2} for wavelength= 1539.6nm, $R_4 = R_{13}$ = –2.43×10^{-2} for wavelength= 1540nm, $R_5 = R_{12}$ = –2.34×10^{-2} for wavelength= 1540.4nm, $R_6 = R_{11}$ = –2.24×10^{-2} for wavelength= 1540.8nm, $R_7 = R_{10}$ = –2.14×10^{-2} for wavelength= 1541.2nm, $R_8 = R_9$ = –2.04×10^{-2} for wavelength= 1541.6nm, $R_{25} = R_{24}$ = –1.95×10^{-2} for wavelength= 1542nm, $R_{26} = R_{23}$ = –1.85×10^{-2} for wavelength= 1542.4nm, $R_{27} = R_{22}$ = –1.75×10^{-2} for wavelength= 1542.8nm, $R_{28} = R_{21}$ = –1.65×10^{-2} for wavelength= 1543.2nm, $R_{29} = R_{20}$ = –1.56×10^{-2} for wavelength= 1543.6nm, $R_{30} = R_{19}$ = –1.46×10^{-2} for wavelength= 1544nm, $R_{31} = R_{18}$ = –1.36×10^{-2} for wavelength= 1544.4nm, $R_{32} = R_{17}$ = –1.26×10^{-2} for wavelength= 1544.8nm.

Fig. 3-31 shows the simulation results of (a)-(d) for ITU wavelength from 1538.8nm to 1540nm launching into 16×16 microring routing wavelength switch from input port1 to input port4. Fig. 3-31(a) show a light wavelength 1538.8nm propagate from input1 to output16 and the transmittance value of the output16 is –13.745 dBm. Fig. 3-31(b) show a light wavelength 1539.2nm propagate from input2 to output15 and the transmittance value of the output15 is –11.321dBm. Fig. 3-31(c) show a light wavelength 1539.6nm propagate from input3 to output14 and the transmittance value of the output14 is –9.934dBm. Fig. 3-31(d) show a light wavelength 1540nm propagate from input4 to output13 and the transmittance value of the output13 is –8.545dBm.

Fig. 3-32 shows the simulation results of (a)-(d) for ITU wavelength from 1540.4nm to 1541.6nm launching into 16×16 microring routing wavelength switch from input port5 to input port8. Fig. 3-32(a) show a light wavelength 1540.4nm propagate from input5 to output12 and the transmittance value of the output12 is 7.219dBm. Fig. 3-32(b) show a light wavelength 1540.8nm propagate from input6 to output11 and the transmittance value of the output11 is –5.834dBm. Fig. 3-32(c) show a light wavelength 1541.2nm propagate from input7 to output10 and the transmittance value of the output10 is –4.418dBm. Fig. 3-32(d) show a light wavelength 1541.6nm propagate from input8 to output9 and the transmittance value of the output9 is –3.920dBm.

Fig. 3-33 shows the simulation results of (a)-(d) for ITU wavelength from 1542nm to 1543.2nm launching into 16×16 microring routing wavelength switch from input port1 to input port4. Fig. 3-33(a) show a light wavelength 1542nm propagate from input9 to output8 and the transmittance value of the output8 is –4.144dBm. Fig. 3-33(b) show a light wavelength 1542.4nm propagate from input10 to output7 and the transmittance value of the output7 is –4.878dBm. Fig. 3-33(c) show a light wavelength 1542.8nm propagate from input11 to output6 and the transmittance value of the output6 is –5.734dBm. Fig. 3-33(d) show a light wavelength 1543.2nm propagate from input12 to output5 and the transmittance value of the output5 is –7.252dBm.

Fig. 3-34 shows the simulation results for ITU wavelength from 1543.6nm to 1544.8nm launching into 16×16 microring routing wavelength switch from input port13 to input port16. Fig. 3-34(a) show a light wavelength 1543.6nm propagate from input13 to output4 and the transmittance value of the output4 is –8.355dBm. Fig. 3-34(b) show a light wavelength 1544nm propagate from input14 to output3 and the transmittance value of the output3 is –9.734dBm. Fig. 3-34(c) show a light wavelength 1544.4nm propagate from input15 to output2 and the transmittance value of the output2 is –11.221dBm. Fig. 3-34(d) show a light wavelength 1544.8nm propagate from input16 to output1 and the transmittance value of the output1 is –13.645dBm. In addition to before we mentioned, we also simulate the four wavelength individual launching into input port. Fig. 3-35 shows the output power at individual output channel with different refractive index change for the four wavelength individual launching into input port 4. Fig. 3-36 shows the output power at individual output channel with different refractive index change for the four wavelength individual launching into input port 8. Fig. 3-37 shows the output power at individual output channel with different refractive index change for the four wavelength individual launching into input port 12. Fig. 3-38 shows the output power at individual output channel with different refractive index change for the four wavelength individual launching into input port 16. Fig. 3-39 shows the output power at individual 8 output ports with different refractive index change for ITU wavelength launching into 16×16 grid array microring resonator wavelength switch device.

3-3-4 Design and Analysis of 32×32 Optical Routing Wavelength Switch by SOI Microring Resonator

In this section, we design an 32×32 microring cross grid wavelength switching network based on free carrier plasma effect by FDTD method. We simulate the routing effect from arbitrary input to any other out put by controlling the individual ring waveguide refractive index. The optical wavelength switch with adding various voltages on several electrode pad regions to control light signal switching path are also simulated. The size of the 32×32 wavelength switching network is 600μm×30μm. Fig. 3-40 shows the top view of our designed 32×32 optical wavelength switching network with 64 microrings as control elements. With tuning the voltages on several electrode pads and use the different change of refractive index on several regions to control the light wave propagation path. We use the ITU 0.4nm wavelength spacing to launch into the microring optical wavelength switch. In addition to all of the above, we can switch the light wave propagate from one of 32 input channels to one of 32 output channels as aspiration. Fig. 3-41 shows a light wavelength 1540nm launching into input port 8 at our designed 32×32 optical wavelength switching network. Fig. 3-41(a) shows a light wavelength 1540nm propagate from input 8 to output 8 and the transmittance value of the output8 is –1.2342 dBm. With didn't add any voltages on several electrode pads, the light transmit straightly to the output8. Fig. 3-41(b) shows a light wavelength 1540nm propagate from input8 to output16 and the transmittance value of the output16 is –8.752 dBm. We add voltages on several electrode pads such as R_8 and R_{16} and use the change of refractive index (△n=–2.4×10^{-2}) on several regions to control the light wave propagation path. Fig. 3-41(c) shows a light wavelength 1540nm propagate from input8 to output24 and the transmittance value of the output24 is –16.534dBm. We add voltages on several fingered electrode pads such as R_8 and R_{24} and use the change of refractive index (△n=–2.4×10^{-2}) on several regions to control the light wave propagation path. Fig. 3-41(d) shows a light wavelength 1540nm propagate from input8 to output32 and the transmittance value of the output32 is –25.052dBm. We add voltages on several fingered electrode pads such as R_8 and R_{32} and use the change of refractive index (△n=–2.4×10^{-2}) on several regions to control the light wave propagation path.

Fig. 3-42 shows a light wavelength 1540nm launching into input port 16 at our designed 32×32 optical wavelength switching network. Fig. 3-42(a) shows a light wavelength 1540nm propagate from input16 to output8 and the transmittance value of the output8 is –9.334dBm. We add voltages on several electrode pads such as R_{40} and R_{33} and use the change of refractive index (△n=–2.4×10^{-2}) on several regions to control the light wave propagation path. Fig. 3-42(b) shows a light wavelength 1540nm propagate from input16 to output16 and the transmittance value of the output16 is –1.252dBm. With didn't add any voltages on several electrode pads, the light transmit straightly to the output16. Fig. 3-42(c) shows a light wavelength 1540nm propagate from input16 to output24 and the transmittance value of the output24 is –10.334dBm. We add voltages on several fingered electrode pads such as R_{16} and R_{24} and use the change of refractive index (△n=–2.4×10^{-2}) on several regions to control the light wave propagation path. Fig. 3-42(d) shows a light wavelength 1540nm propagate from input16 to output32 and the transmittance value of the output32 is –16.252dBm. We add voltages on several fingered electrode pads such as R_{16} and R_{32} and use the change of refractive index (△n=–2.4×10^{-2}) on several regions to control the light wave propagation path.

Fig. 3-43 shows a light wavelength 1540nm launching into input port 24 at our designed 32×32 optical wavelength switching network. Fig. 3-43(a) shows a light wavelength 1540nm propagate from input24 to output8 and the transmittance value of the output8 is –16.729dBm. We add voltages on several electrode pads such as R_{56} and R_{40} and use the change of refractive index (△n=–2.4×10^{-2}) on several regions to control the light wave propagation path. Fig. 3-43(b) shows a light wavelength 1540nm propagate from input24 to output16 and the transmittance value of the output16 is –9.034dBm. We add voltages on several fingered electrode pads such as R_{56} and R_{48} and use the change of refractive index (△n=–2.4×10^{-2}) on several regions to control the light wave propagation path. Fig. 3-43(c) shows a light wavelength 1540nm propagate from input24 to output24 and the transmittance value of the output24 is –1.252dBm. With didn't add any voltages on several electrode pads, the light transmit straightly to the output24. Fig. 3-43(d) shows a light wavelength 1540nm propagate from input24 to output32 and the transmittance value of the output32 is –10.287dBm. We add voltages on several fingered electrode pads such as R_{24} and R_{32} and use the change of refractive index (△n=–2.4×10^{-2}) on several regions to control the light wave propagation path.

Fig. 3-44 shows a light wavelength 1540nm launching into input port

32 at our designed 32×32 optical wavelength switching network. Fig. 3-44(a) shows a light wavelength 1540nm propagate from input32 to output8 and the transmittance value of the output8 is –22.023dBm. We add voltages on several electrode pads such as R_{64} and R_{40} and use the change of refractive index (△n=–2.4×10^{-2}) on several regions to control the light wave propagation path. Fig. 3-44(b) shows a light wavelength 1540nm propagate from input32 to output16 and the transmittance value of the output16 is –16.438dBm. We add voltages on several fingered electrode pads such as R_{64} and R_{48} and use the change of refractive index (△n=–2.4×10^{-2}) on several regions to control the light wave propagation path. Fig. 3-44(c) shows a light wavelength 1540nm propagate from input32 to output24 and the transmittance value of the output24 is –9.548dBm. We add voltages on several fingered electrode pads such as R_{64} and R_{56} and use the change of refractive index (△n=–2.4×10^{-2}) on several regions to control the light wave propagation path. Fig. 3-44(d) shows a light wavelength 1540nm propagate from input32 to output32 and the transmittance value of the output8 is –1.157dBm. With didn't add any voltages on several electrode pads, the light transmit straightly to the output32.

Fig. 3-45 and Fig. 3-46 shows an ITU light wavelength from 1537.2nm to 1549.6nm launching into each input port from channel1 to channel32 at our designed 32×32 microring routing wavelength switch individually. The total number of our input wavelength is 32 and the channel spacing is 0.4nm. In this case, we add voltages on several electrode pads and use the various change of refractive index from –9.75×10^{-4} to –3.12×10^{-2} on several regions to control the light wave propagation path. The regions of adding voltages and the change of refractive index on several fingered electrode pads such as R_1 = R_{32} = –3.12×10^{-2} for wavelength = 1537.2nm, R_2 = R_{31} = -2.945×10^{-2} for wavelength = 1537.6nm, R_3 = R_{30} = -2.925×10^{-2} for wavelength= 1538nm, R_4 = R_{29} = -2.755×10^{-2} for wavelength= 1538.4nm, R_5 = R_{28} = -2.73×10^{-2} for wavelength= 1538.8nm, R_6 = R_{27} = -2.63×10^{-2} for wavelength= 1539.2nm, R_7 = R_{26} = -2.535×10^{-2} for wavelength= 1539.6nm, R_8 = R_{25} = -2.437×10^{-2} for wavelength= 1540nm, R_9 = R_{24} = -2.34×10^{-2} for wavelength= 1540.4nm, R_{10} = R_{23} = -2.242×10^{-2} for wavelength= 1540.8nm, R_{11} = R_{22} = -2.145×10^{-2} for wavelength= 1541.2nm, R_{12} = R_{21} = -2.047×10^{-2} for wavelength= 1541.6nm, R_{13} = R_{20} = -1.95×10^{-2} for wavelength= 1542nm, R_{14} = R_{19} = -1.852×10^{-2} for wavelength= 1542.4nm, R_{15} = R_{18} = -1.755×10^{-2} for wavelength= 1542.8nm, R_{16}= R_{17} = -1.657×10^{-2} for wavelength= 1543.2nm. R_{49}=R_{48} = -1.56×10^{-2} for wavelength= 1543.6nm, R_{50} = R_{47} = -1.462×10^{-2} for wavelength= 1544nm, R_{51} = R_{46} = -1.365×10^{-2} for wavelength= 1544.4nm, R_{52} = R_{45} = -1.267×10^{-2} for wavelength= 1544.8nm, R_{53} = R_{44} = -1.17×10^{-2} for wavelength= 1545.2nm, R_{54} = R_{43} = -1.072×10^{-2} for wavelength= 1545.6nm, R_{55} = R_{42} = -9.75×10^{-3} for wavelength= 1546nm, R_{56} = R_{41} = -8.775×10^{-3} for wavelength= 1546.4nm, R_{57} = R_{40} = -7.8×10^{-3} for wavelength= 1546.8nm, R_{58} = R_{39} = -6.825×10^{-3} for wavelength= 1547.2nm, R_{59} = R_{38} = -5.85×10^{-3} for wavelength= 1547.6nm, R_{60} = R_{37} = -4.875×10^{-3} for wavelength= 1548nm, R_{61} = R_{36} = -3.9×10^{-3} for wavelength= 1548.4nm, R_{62} = R_{35} = -2.925×10^{-3} for wavelength= 1548.8nm, R_{63} = R_{34} = -1.95×10^{-3} for wavelength= 1549.2nm, R_{64}= R_{32} = -9.75×10^{-4} for wavelength= 1549.6nm.

Fig. 3-45 shows the simulation results of (a)-(d) for ITU wavelength from 1538.4nm to 1543.2nm launching into 32×32 microring routing wavelength switch from input port4 to input port16. Fig. 3-45(a)show a light wavelength 1538.4nm propagate from input4 to output29 and the transmittance value of the output29 is –23.829dBm. Fig. 3-45(b) show a light wavelength 1540nm propagate from input8 to output25 and the transmittance value of the output25 is –17.344dBm. Fig. 3-45(c) show a light wavelength 1541.6nm propagate from input12 to output21 and the transmittance value of the output21 is –11.729 dBm. Fig. 3-45(d) show a light wavelength 1543.2nm propagate from input16 to output17 and the transmittance value of the output13 is –4.309dBm.

Fig. 3-46 shows the simulation results of (a)-(d) for ITU wavelength from 1544.8nm to 1549.6nm launching into 32×32 microring routing wavelength switch from input port20 to input port32. Fig. 3-46(a) show a light wavelength 1544.8nm propagate from input20 to output13 and the transmittance value of the output12 is –12.145dBm. Fig. 3-46(b) show a light wavelength 1546.4nm propagate from input24 to output9 and the transmittance value of the output9 is –16.209dBm. Fig. 3-46(c) show a light wavelength 1548nm propagate from input28 to output5 and the transmittance value of the output5 is –20.092dBm. Fig. 3-46(d) show a light wavelength 1549.6nm propagate from input32 to output1 and the transmittance value of the output9 is –28.943dBm.

In addition to before we mentioned, we also simulate the other four wavelength individual launching into input port. Fig. 3-47 shows the output power at individual output channel with different refractive index change for the four wavelength individual launching into input port 8. Fig. 3-48 shows the output power at individual output channel with different refractive index change for the four wavelength individual launching into input port 16. Fig. 3-49 shows the output power at individual output channel with different refractive index change for the four wavelength individual launching into input port 24. Fig. 3-50 shows the output power at individual output channel with different refractive index change for the four wavelength individual launching into input port 32. Fig. 3-51 shows the output power at individual 8 output ports with different refractive index change for ITU wavelength launching into 32×32 grid array microring resonator wavelength switch device.

3-4 Discussion of the mathematical Formulation of SNR and Path Loss by N×N grid array Switching Networks

The propagation loss through the cross junction of the switching network is considered the primary loss of the network. The cross junction loss at our designed network is about －12dB. The estimated cross junction loss is directly proportional to the channel number of optical microring switching network through which the optical path passes. Besides, the important issue is the coupling loss of the microring resonator which is on resonance. In our simulation device, there is 1.3874dB loss in one resonance resonator on average. The 2×2 switch device have 2.79 dB loss on average for devices. From before simulations to the cross grid array, we will derived the mathematical formulation to the N×N microring resonator optical routing wavelength switch. Note that in any of the four general configurations, the signal comes out at one output while a crosstalk signal comes out at the other output. Let "m" denote the coupling loss ratio for the single microring resonator which is on resonance. From previous simulation results, the value "m" is about 0.24 .And "T" means the loss ratio which the signal light through the cross junction. From previous simulation results, the value "T" is about 0.06 Let "P_M" denote the power of the output signal and the "X" means the power of the crosstalk signal and we set the input power are all the same "P_N" =P. The sign "M" and "N" means the M_{th} output channel and N_{th} input channel. Wherever the both input channels of a 2×2 optical wavelength switch may be active at any given time, the switching cases are possible configuration. When the light signal is set for bar state for the 2×2 optical wavelength switch from input1 to output1 or input2 to output2, the output power at output1 P_1 is: $P_1(P_2) = P_{in}(1-T)^2$. The Path loss is $P_{in} \cdot T^2$ When the light signal is set for cross state for the 2×2 optical wavelength switch from input1 to output2 or input2 to output1, the path loss at output2 P_2 is: $P_2(P_1) = P_{in}(1-m)^2(1-T)^3$. The Path loss is $P_{in} \cdot m^2 \cdot T^3$. For the N×N optical wavelength switch case we also can derive the path loss formulations as following shows. As the signal light is input from N_{th} input channel to the N_{th} output channel, the output power at N_{th} channel is $P_N = P_{in}(1-T)^2$ and the path loss is $P_{in} \cdot T^2$. The crosstalk for the 2×2 optical wavelength switch is $P_{in}\left(\frac{T}{2}\right)^2(1-T)$. As the signal light is input from N_{th} input channel to the M_{th} output channel, the output power at N_{th} channel is $P_M = P_{in}(1-m)^2(1-T)^{(|M-N|+2)}$ and the path loss is :

$$P_{in} \cdot m^2 \cdot T^{(|M-N|+2)}. \tag{3-8}$$

The crosstalk for the N×N optical wavelength switch is

$$P_{crosstalk} = P_{in}\left(\frac{T}{2}\right)^2 (1-T)^N \quad \text{(N=2,4,8,16,32).} \tag{3-9}$$

$$SNR = 10\log_{10}\frac{P_{in}}{P_{crosstalk}} = 10\log_{10}\frac{P_{in}}{\left(P_{in}\left(\frac{T}{2}\right)^2 (1-T)^N\right)} = 10\log_{10}\frac{1}{\left(\frac{T}{2}\right)^2 (1-T)^N} \tag{3-10}$$

Fig. 3-53 shows the relation between SNR and output port channel with different gap from Eqs. 3-10.

3-5 Conclusions

Microring resonators have advantages which make them desirable for Very Large Scale Integrated Photonic Circuits. In ring resonator based devices, the rings are the wavelength selective elements, while the bus waveguides are simply optical conduits that interconnect rings among themselves or to the outside world. In this chapter we have simulate the N×N cross grid array microring resonator. We successfully reduce the size of 32×32 optical cross connect (OXC) to 600×30μm. We simulate the routing behavior to apply in the optical cross connect network. The main loss is due to the junction scattering loss and the coupling loss. But the SNR is low enough to apply in the network. For junction scattering induced cross-talk when bus waveguides cross, while independently optimizing the ring resonator for compactness and low bending loss. It also allows for precision control of the ring-to-waveguide that be decided what wavelength routed to port. In final section, we have derived the formulation to the N×N cross grid array of microring resonator and we will applied this simulation to the optical communication network such as Fig. 3-52 shows.

.

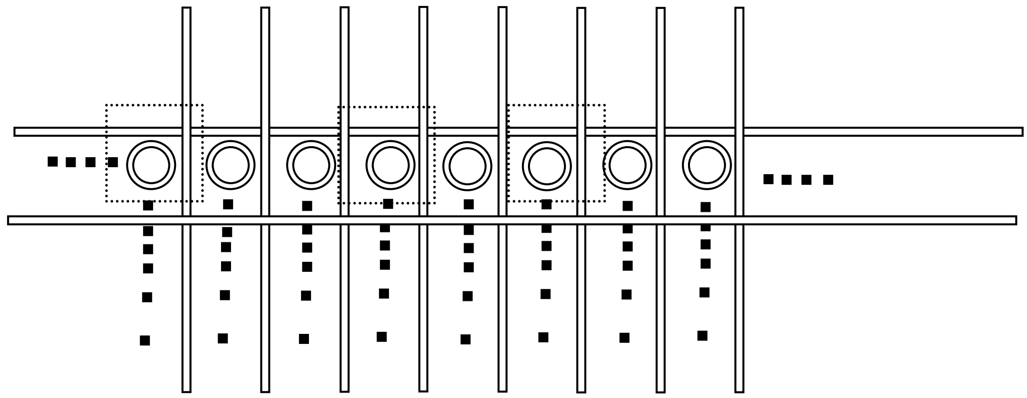

Fig. 3-1 Schematic Diagram of Grid Array Microring Resonator

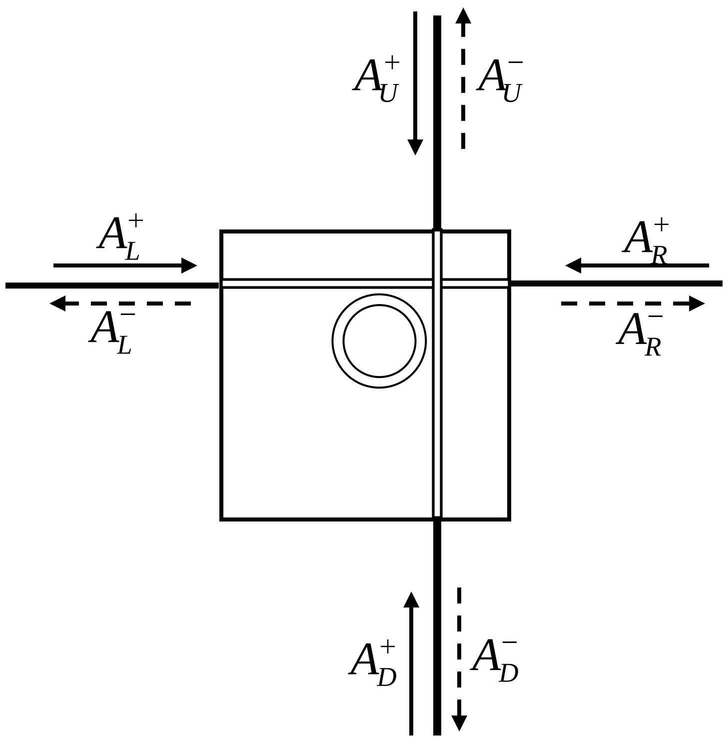

Fig. 3-2 Illustration of Incident and scattered amplitudes at a single cross-grid node.

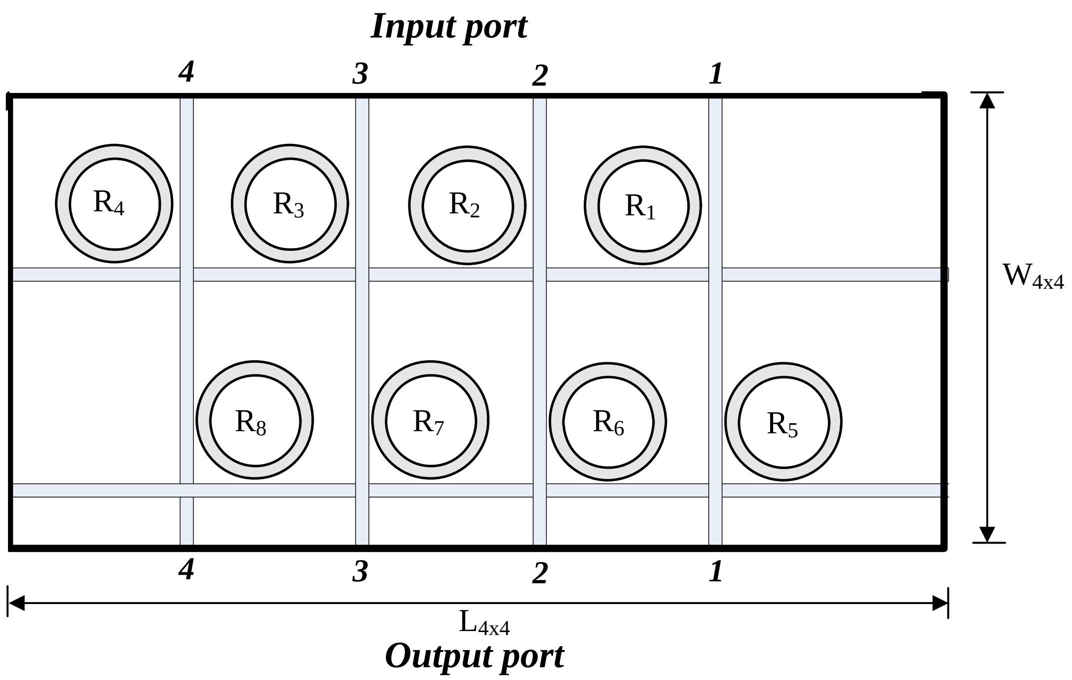

Fig. 3-3 Schematic Diagram of 4×4 Grid Array Microring Resonator Wavelength Switch

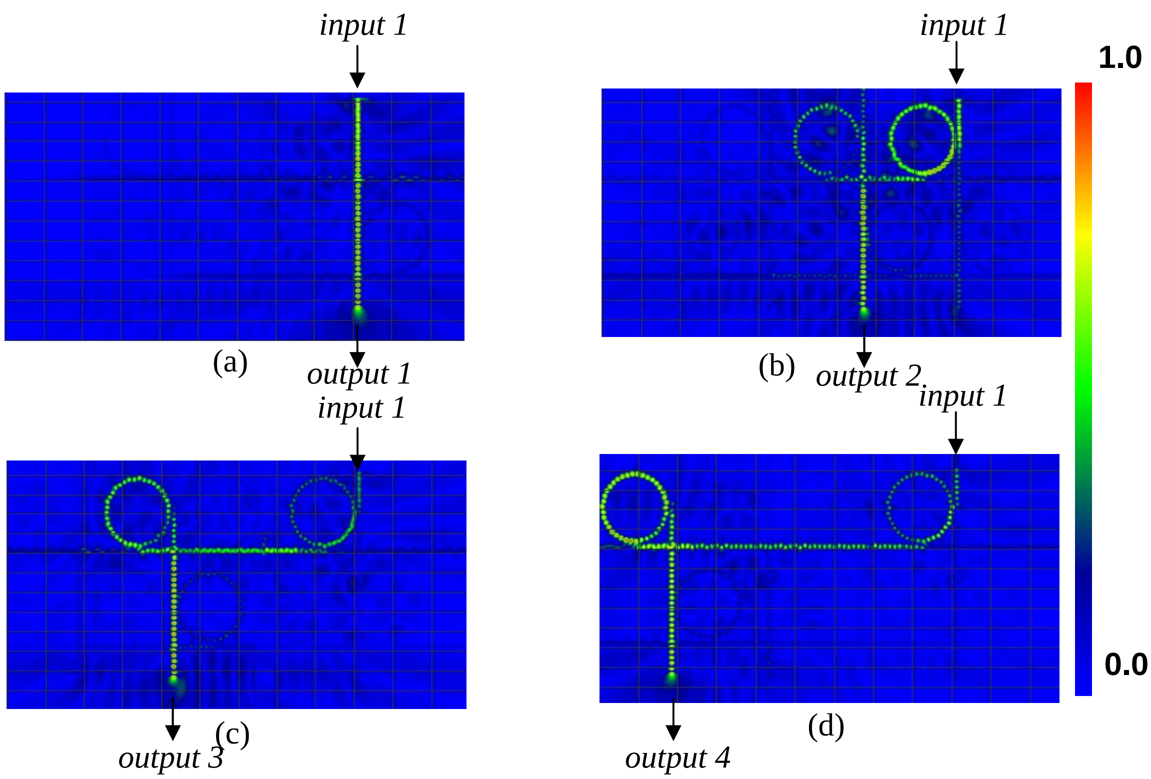

Fig. 3-4 The simulation results of (*a*) output port 1, (*b*) output port 2, (*c*) output port 3, (*d*) output port 4 for the wavelength 1540 nm launching into input port 1 at 4×4 grid Array microring resonator wavelength switch with $\Delta n = -2.4\times10^{-2}$

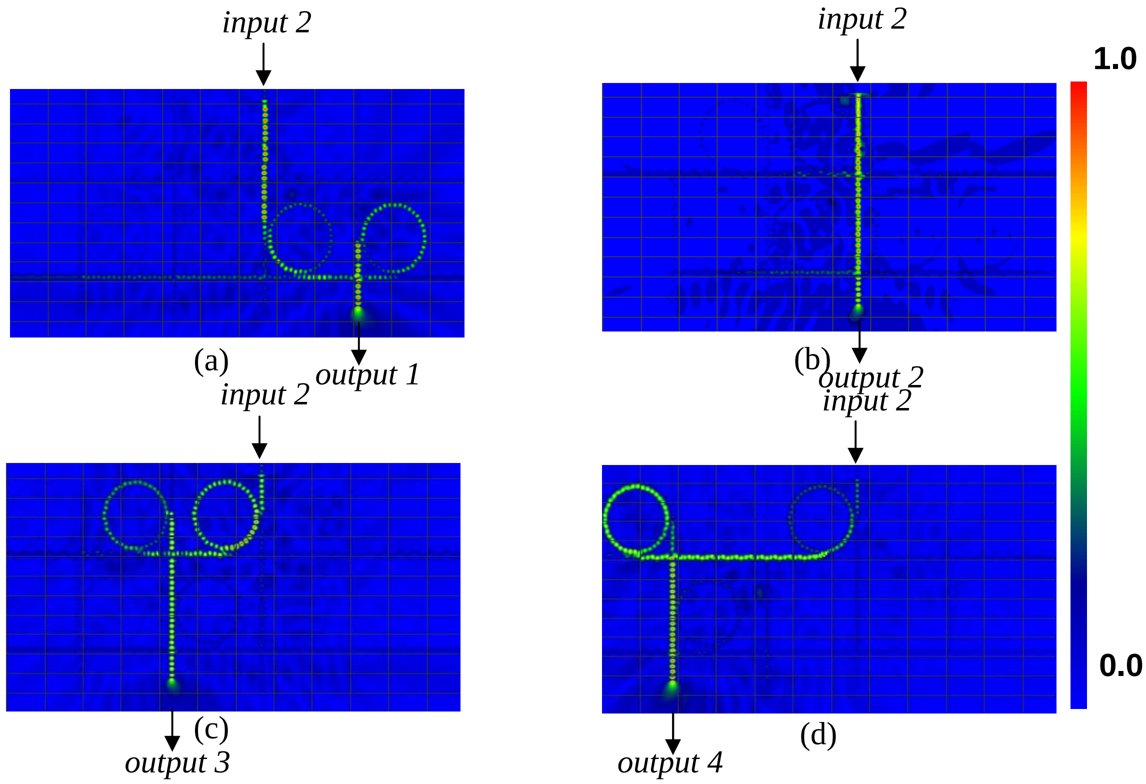

Fig. 3-5 The simulation results of (*a*) output port 1, (*b*) output port 2, (*c*) output port 3, (*d*) output port 4 for the wavelength 1540 nm launching into input port 2 at 4×4 grid array microring resonator wavelength switch with $\Delta n = -2.4\times10^{-2}$

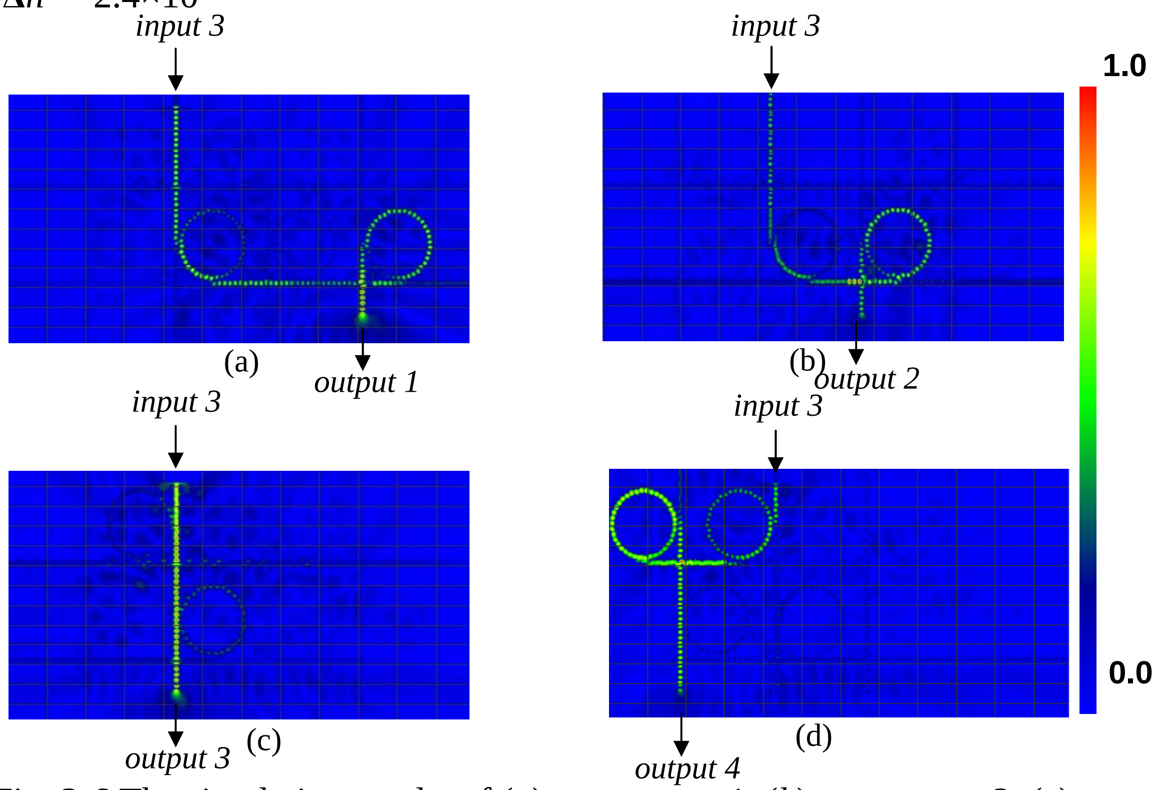

Fig. 3-6 The simulation results of (*a*) output port 1, (*b*) output port 2, (*c*) output port 3, (*d*) output port 4 for the wavelength 1540 nm launching into input port 3 at 4×4 grid array microring resonator wavelength switch with $\Delta n = -2.4\times10^{-2}$

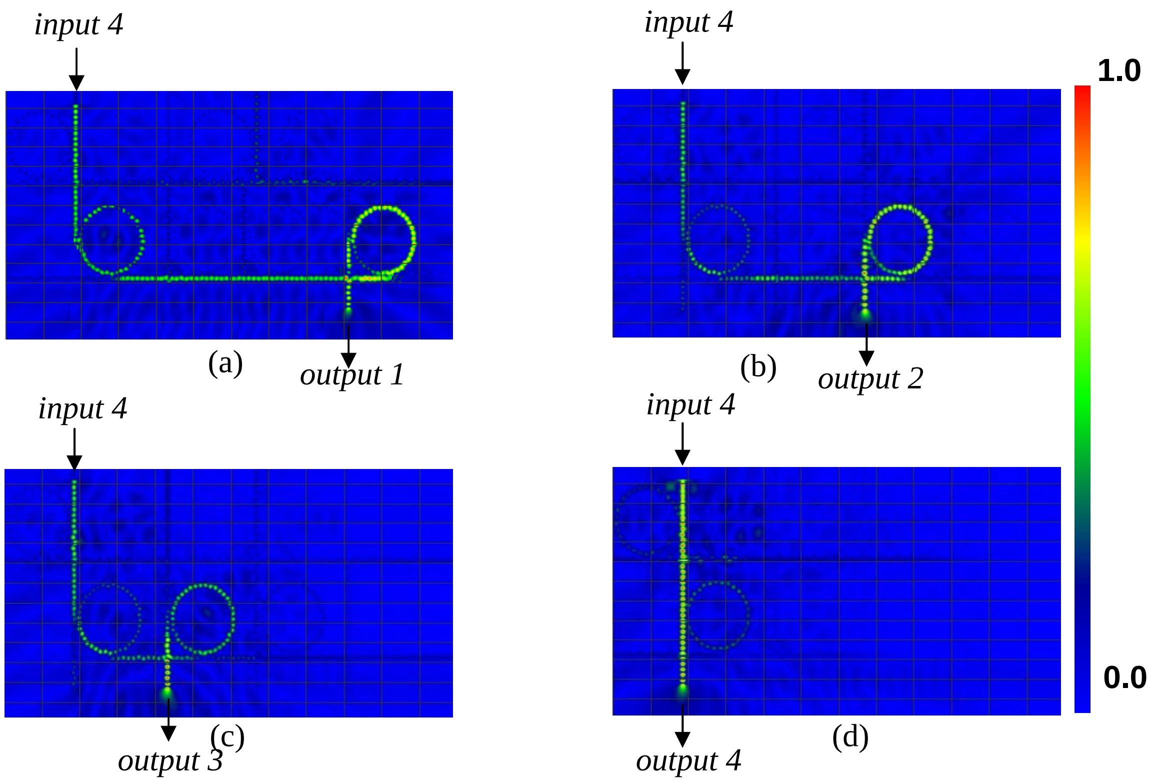

Fig. 3-7 The simulation results of (*a*) output port 1, (*b*) output port 2, (*c*) output port 3, (*d*) output port 4 for the wavelength 1540 nm launching into input port 4 at 4×4 grid array microring resonator wavelength switch with $\Delta n = -2.4\times10^{-2}$

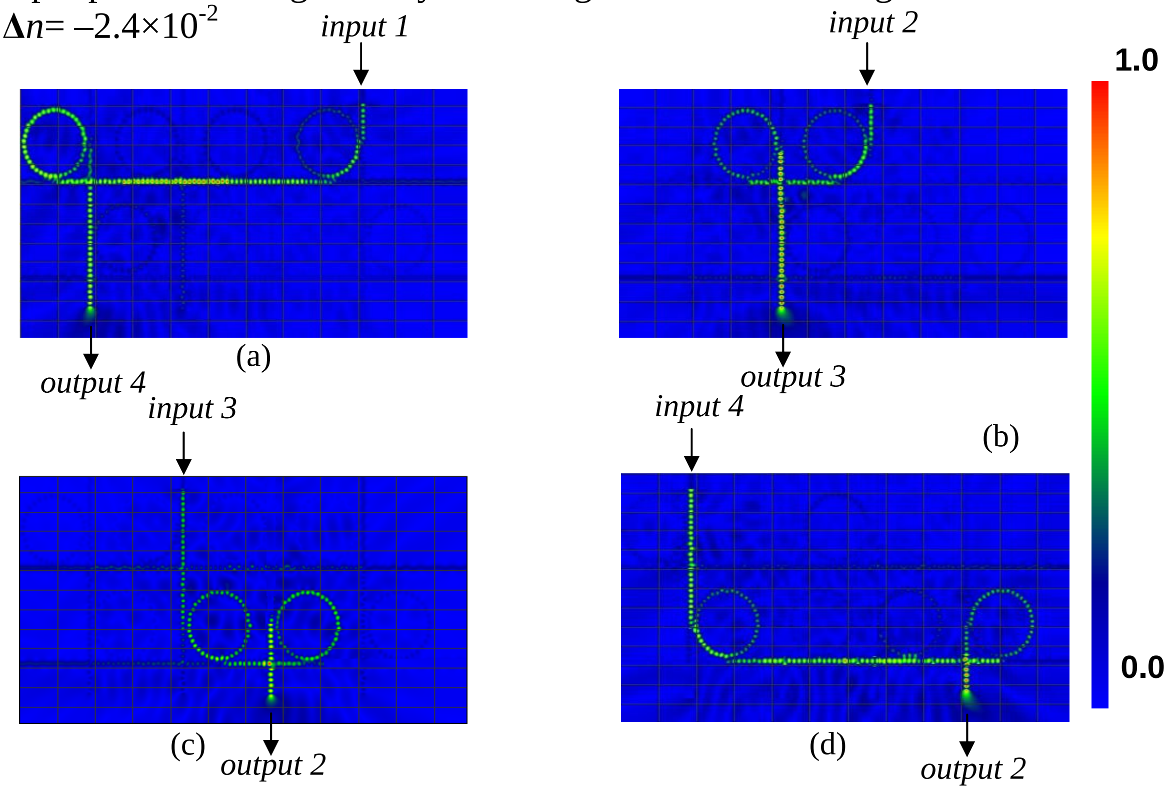

Fig. 3-8 The simulation results of (a)-(d) for ITU wavelength launching into 4×4 grid array microring resonator wavelength switch from input port 1 to input port 4

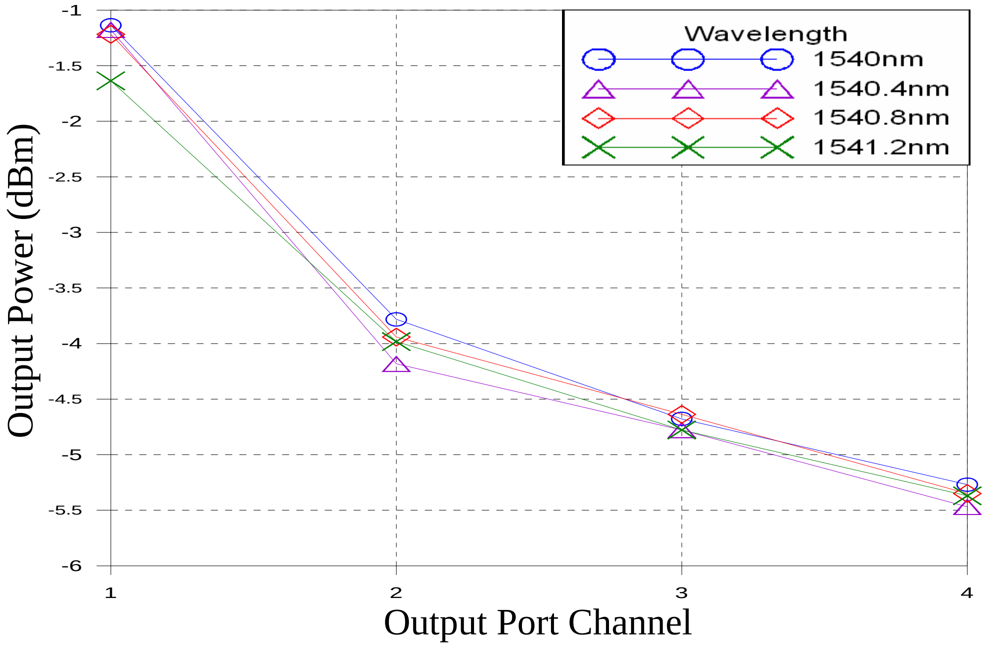

Fig. 3-9 The output power at individual output channel with different refractive index change for the four wavelength individual launching into input port 1

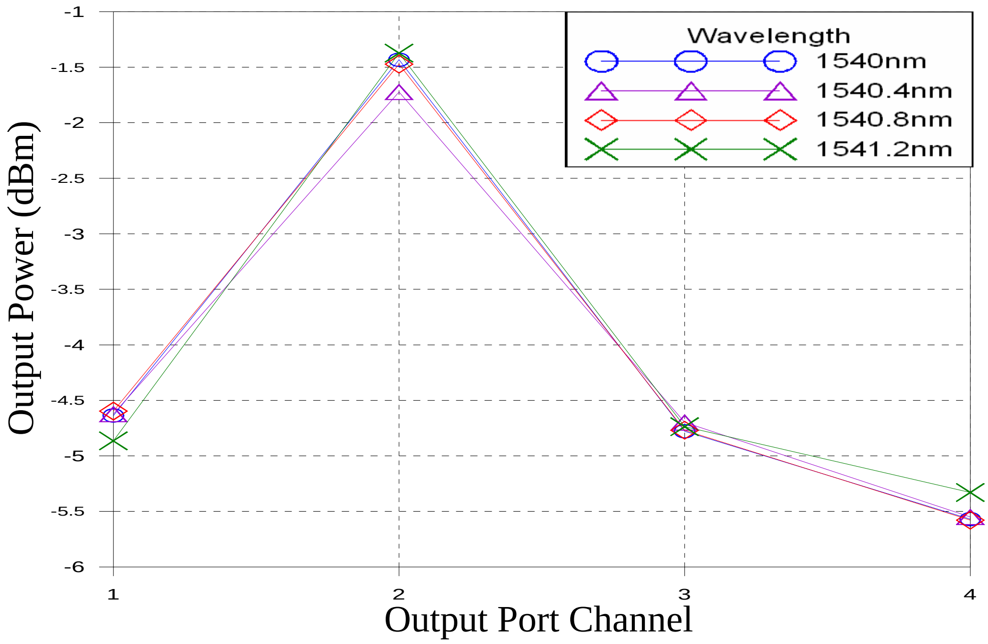

Fig. 3-10 The output power at individual output channel with different refractive index change for the four wavelength individual launching into input port 2

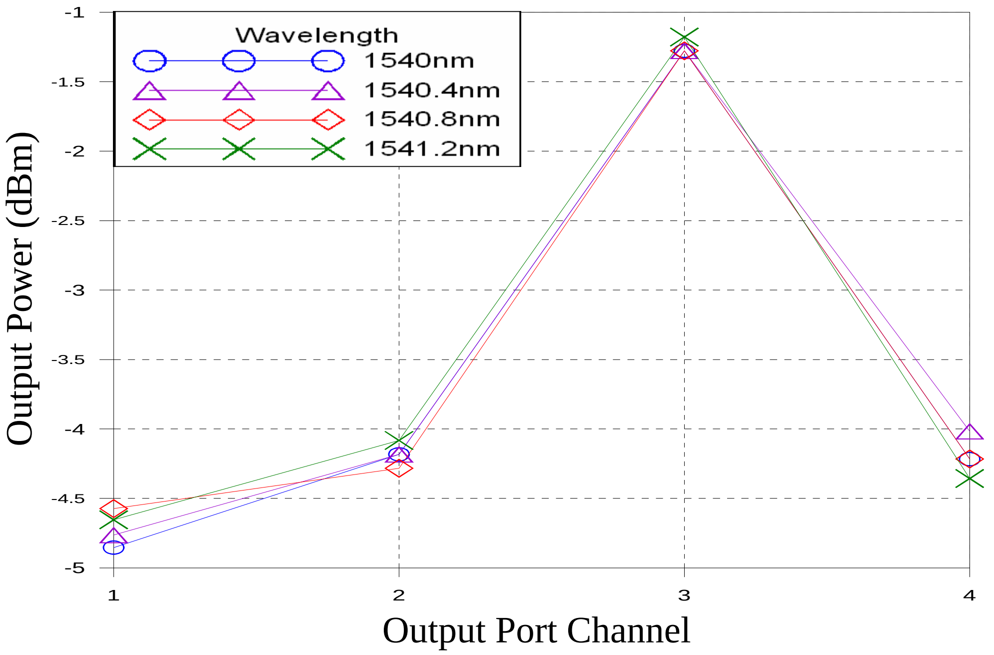

Fig. 3-11 The output power at individual output channel with different refractive index change for the four wavelength individual launching into input port 3

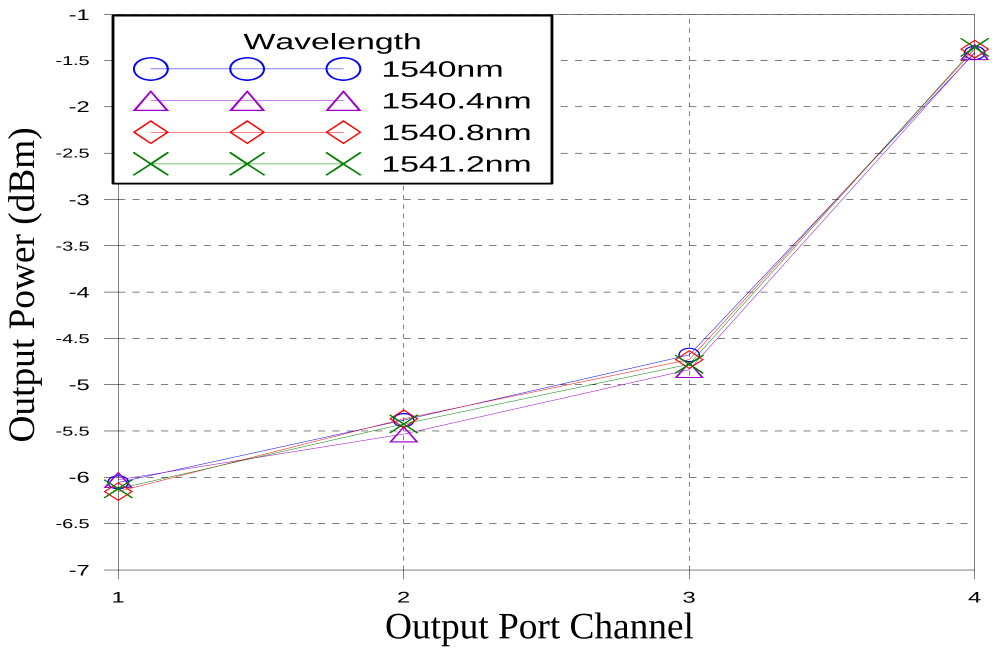

Fig. 3-12 The output power at individual output channel with different refractive index change for the four wavelength individual launching into input port 4

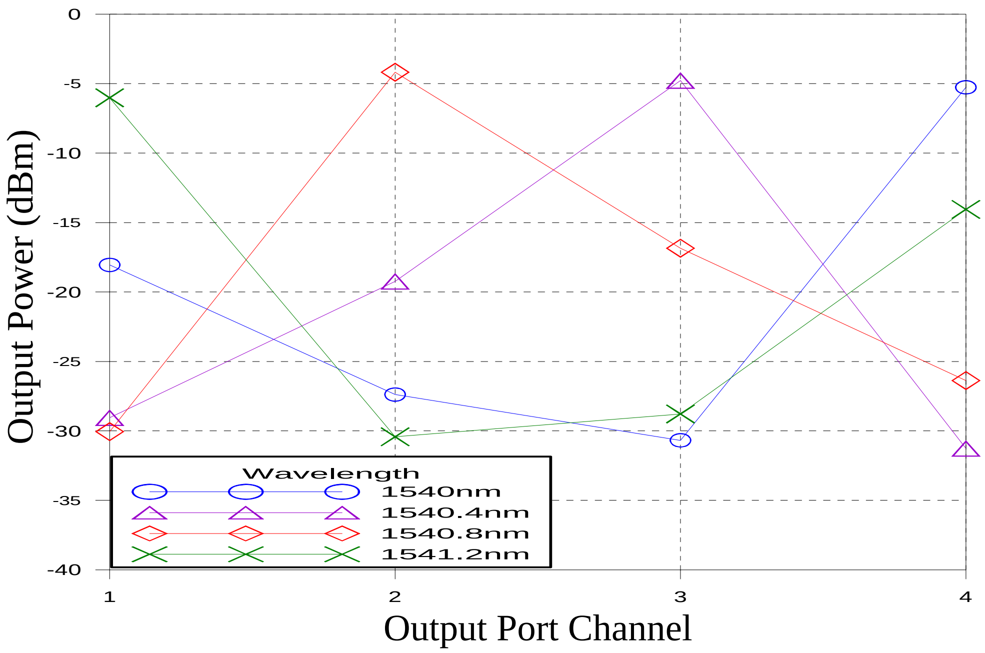

Fig. 3-13 The output power at individual 4 output ports with different refractive index change for ITU wavelength launching into switch device

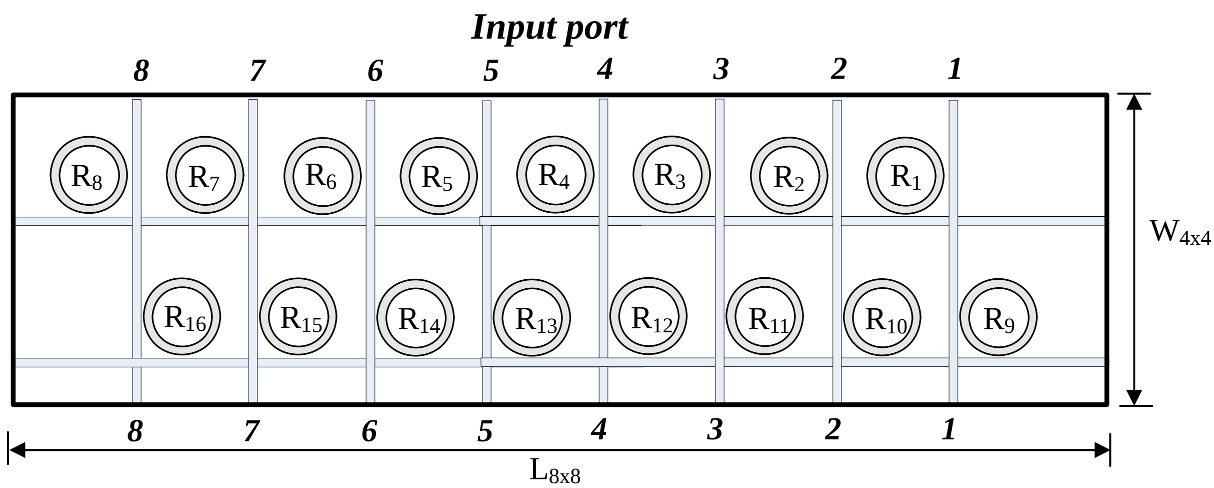

Fig. 3-14 Schematic Diagram of 8×8 Grid Array Microring Resonator Wavelength Switch

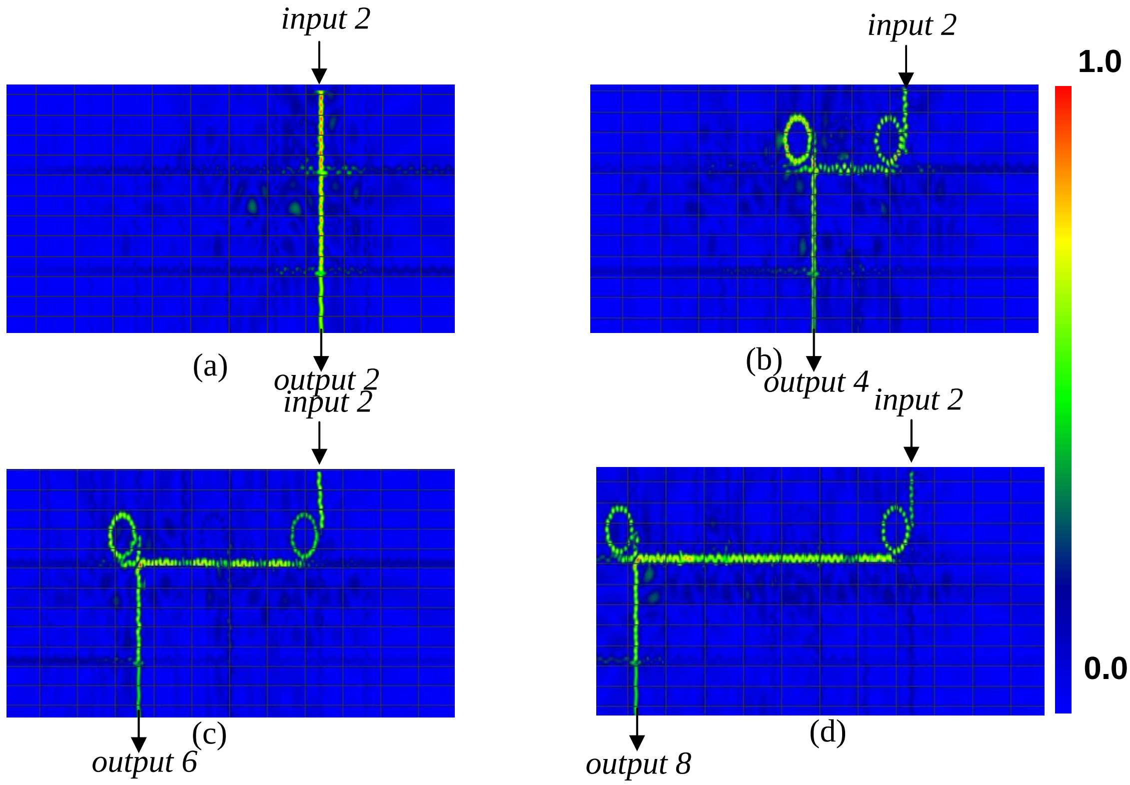

Fig. 3-15 The simulation results of (*a*) output port 2, (*b*) output port 4, (*c*) output port 6, (*d*) output port 8 for the wavelength 1540 nm launching into input port 2 at 8×8 grid array microring resonator wavelength switch with $\Delta n = -2.4\times10^{-2}$

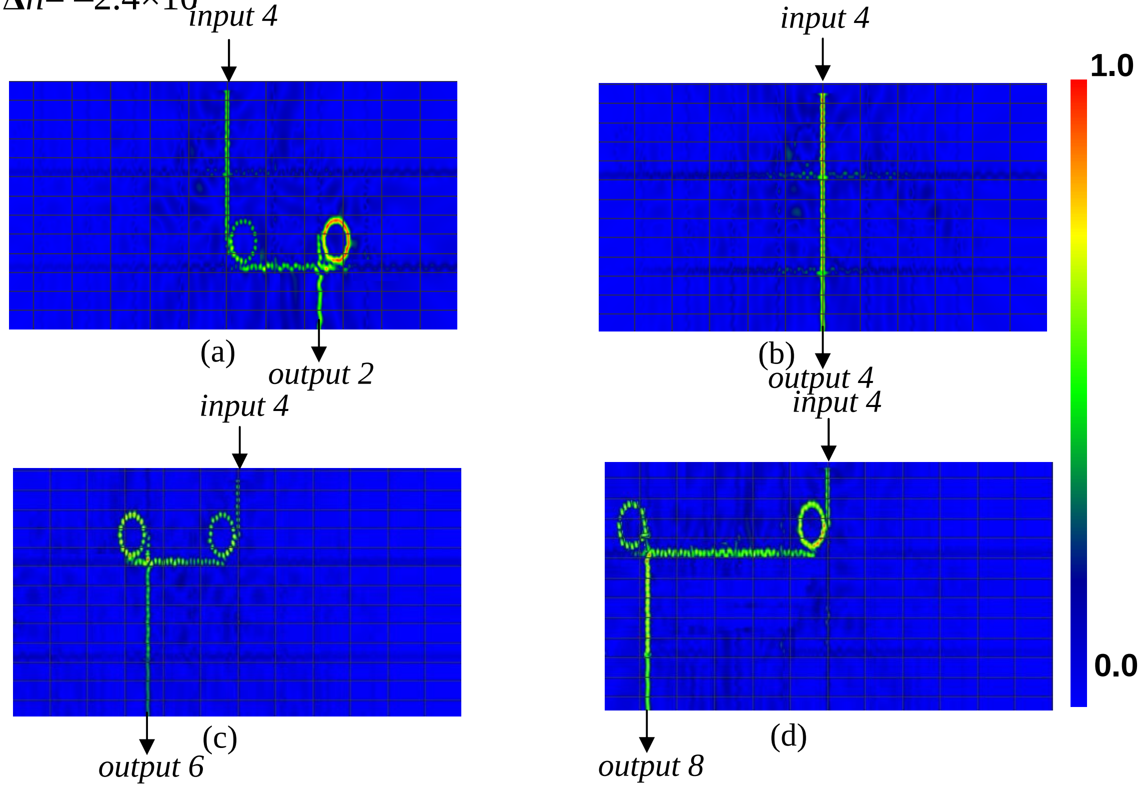

Fig. 3-16 The simulation results of (*a*) output port 2, (*b*) output port 4, (*c*) output port 6, (*d*) output port 8 for the wavelength 1540 nm launching into input port 4 at 8×8 grid array microring resonator wavelength switch with $\Delta n = -2.4\times10^{-2}$

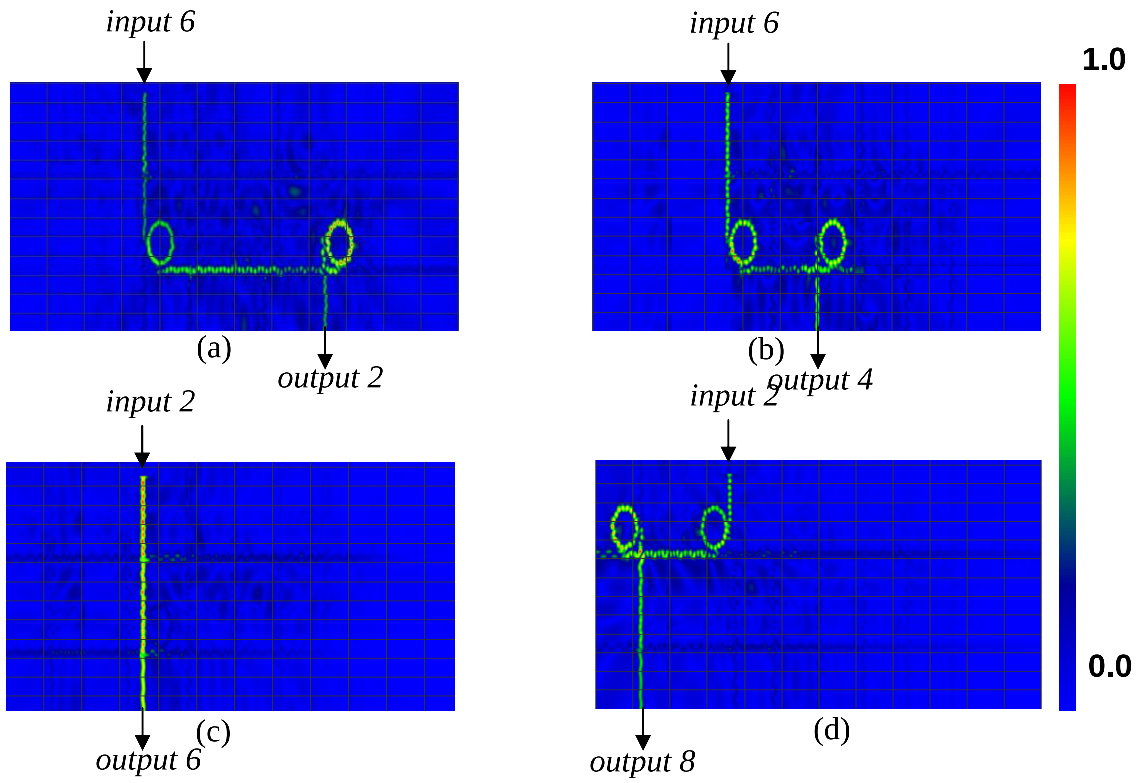

Fig. 3-17 The simulation results of (*a*) output port 2, (*b*) output port 4, (*c*) output port 6, (*d*) output port 8 for the wavelength 1540 nm launching into input port 6 at 8×8 grid array microring resonator wavelength switch with $\Delta n = -2.4\times10^{-2}$

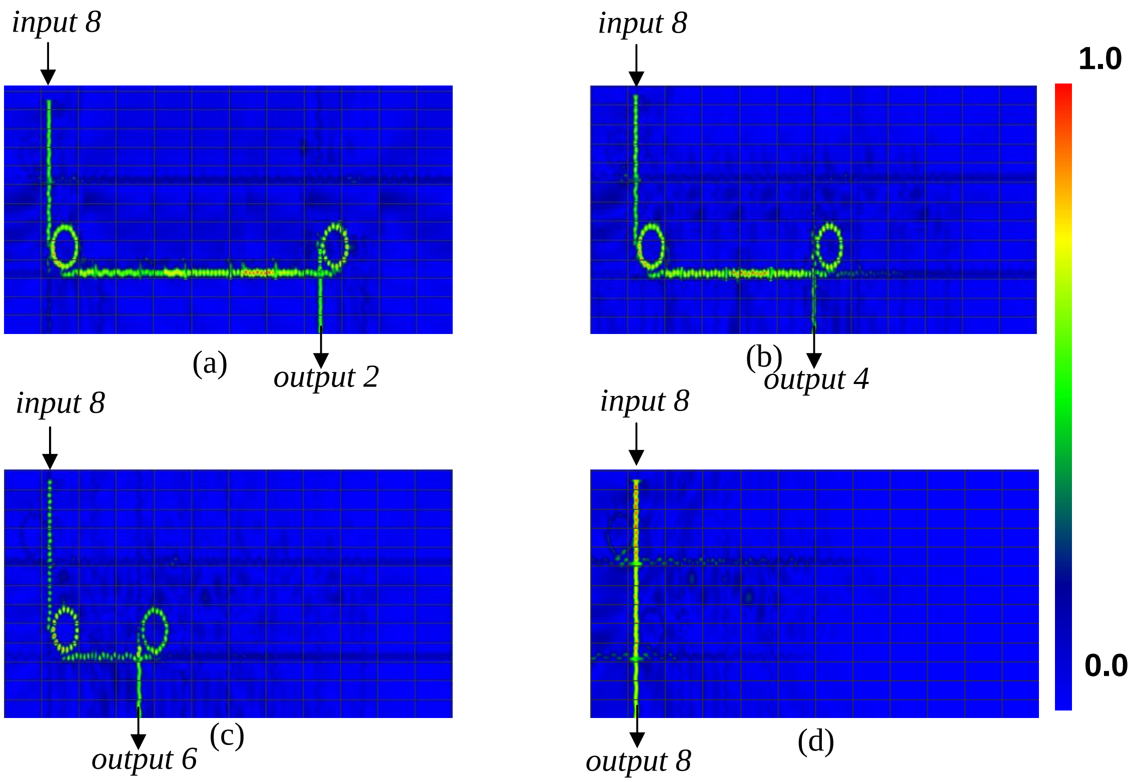

Fig. 3-18 The simulation results of (*a*) output port 2, (*b*) output port 4, (*c*) output port 6, (*d*) output port 8 for the wavelength 1540 nm launching into input port 8 at 8×8 grid array microring resonator wavelength switch with $\Delta n = -2.4\times10^{-2}$

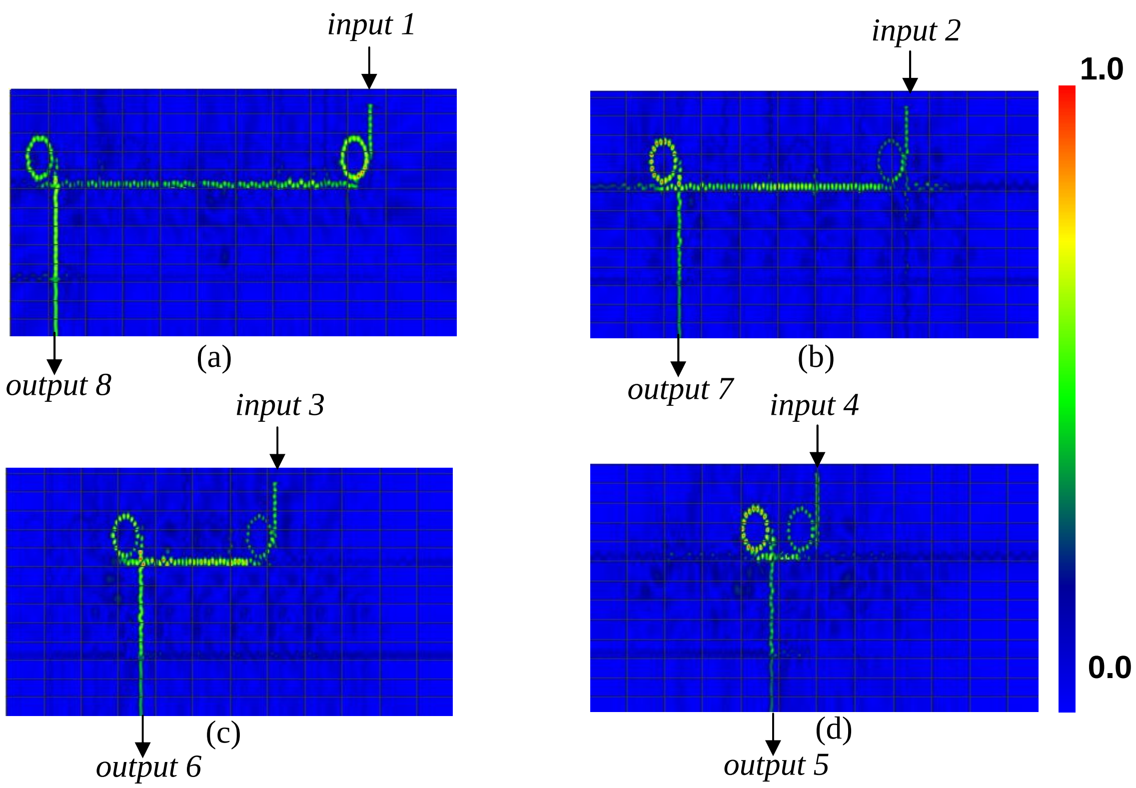

Fig. 3-19 The simulation results of (a)-(d) for ITU wavelength launching into 8×8 grid array microring resonator wavelength switch from input port 1 to input port 4

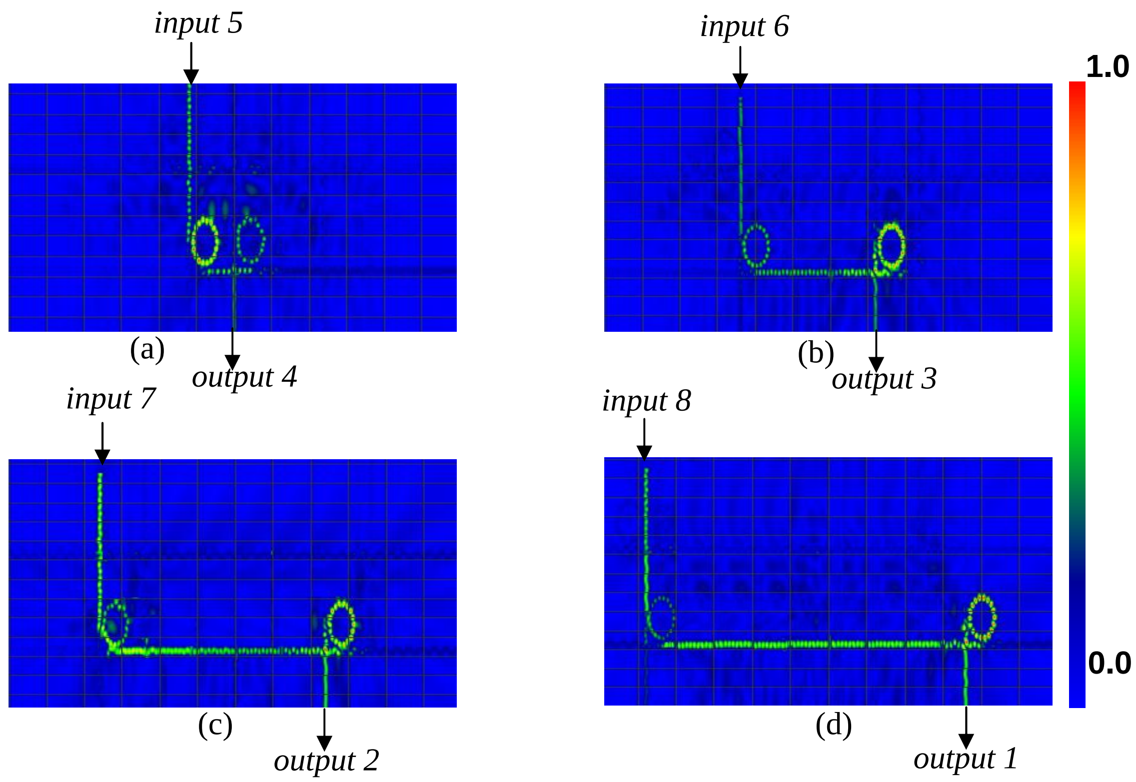

Fig. 3-20 The simulation results of (a)-(d) for ITU wavelength launching into 8×8 grid array microring resonator wavelength switch from input port 5 to input port 8

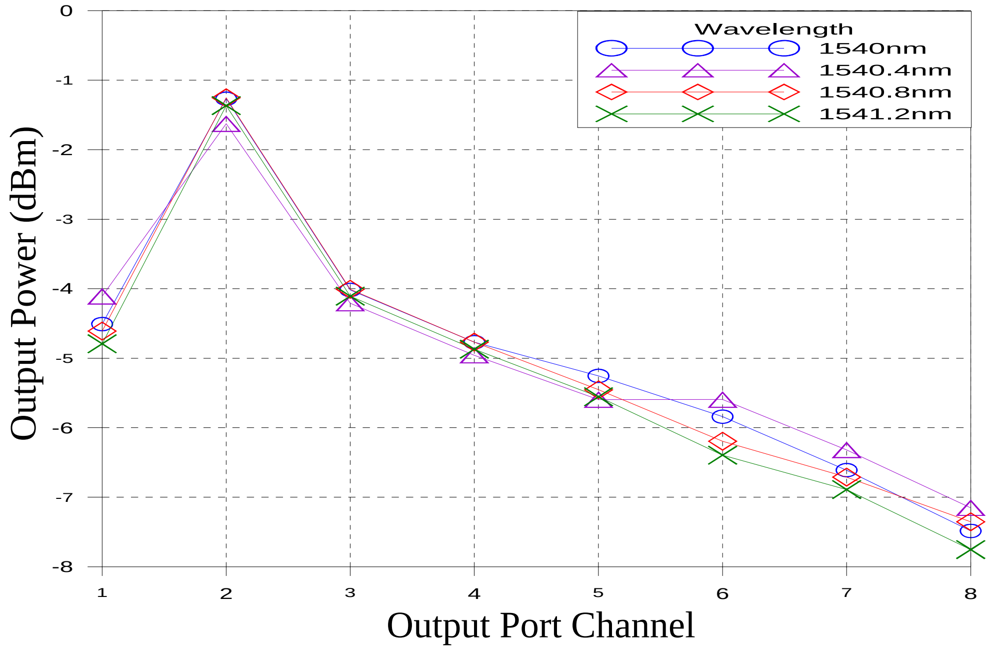

Fig. 3-21 The output power at individual output channel with different refractive index change for the four wavelength individual launching into 8×8 grid array microring resonator wavelength switch input port 2

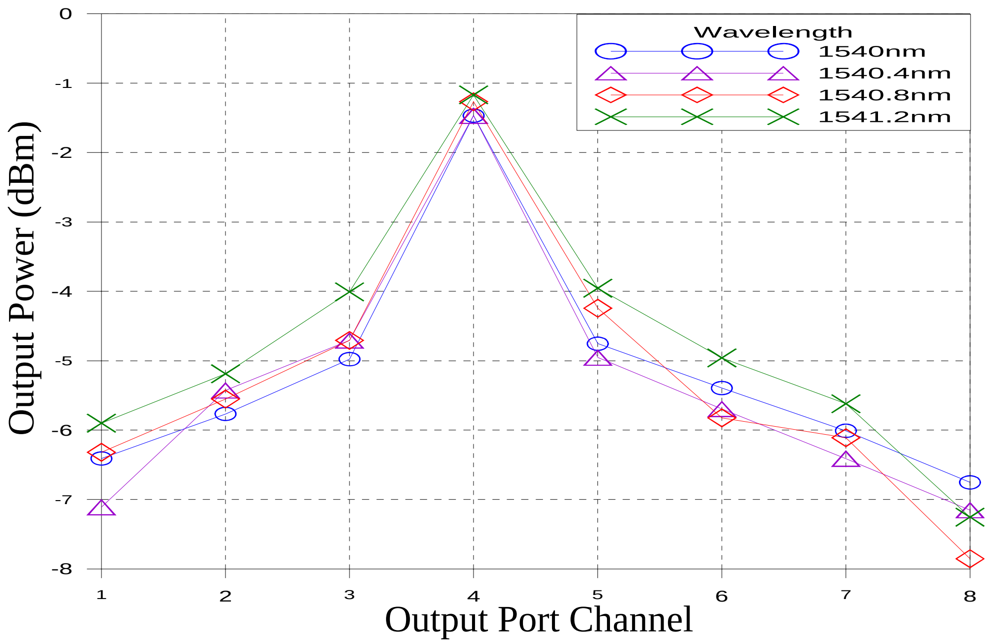

Fig. 3-22 The output power at individual output channel with different refractive index change for the four wavelength individual launching into 8×8 grid array microring resonator wavelength switch input port 4

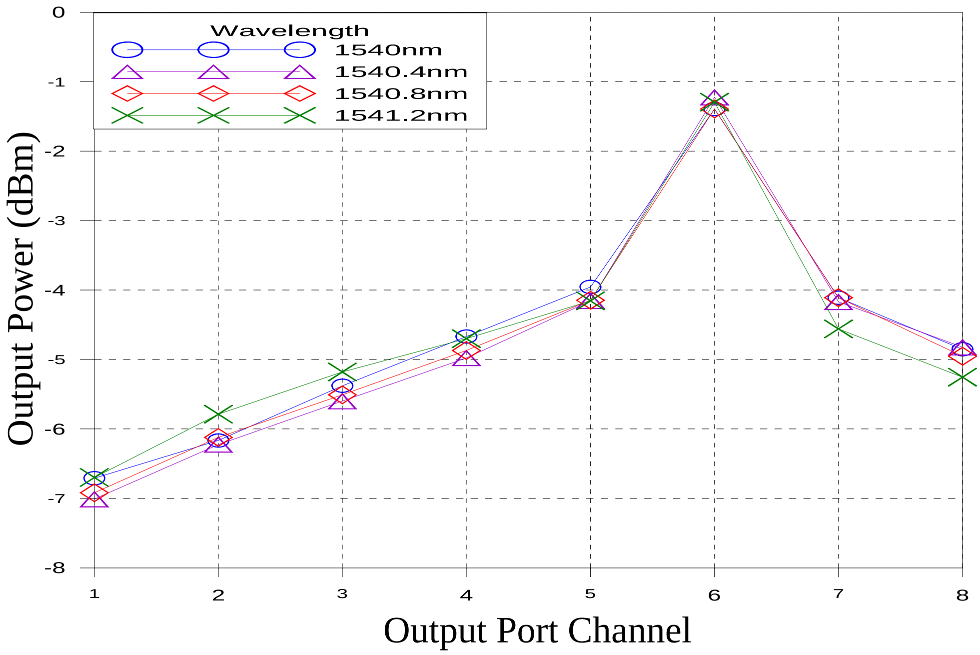

Fig. 3-23 The output power at individual output channel with different refractive index change for the four wavelength individual launching into 8×8 grid array microring resonator wavelength switch input port 6

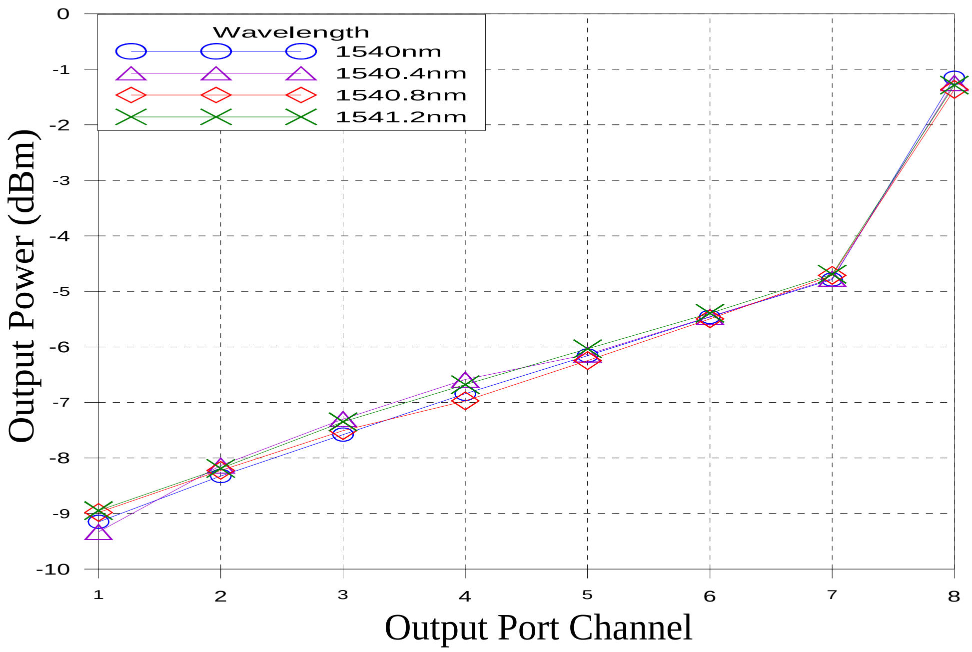

Fig. 3-24 The output power at individual output channel with different refractive index change for the four wavelength individual launching into 8×8 grid array microring resonator wavelength switch input port 8

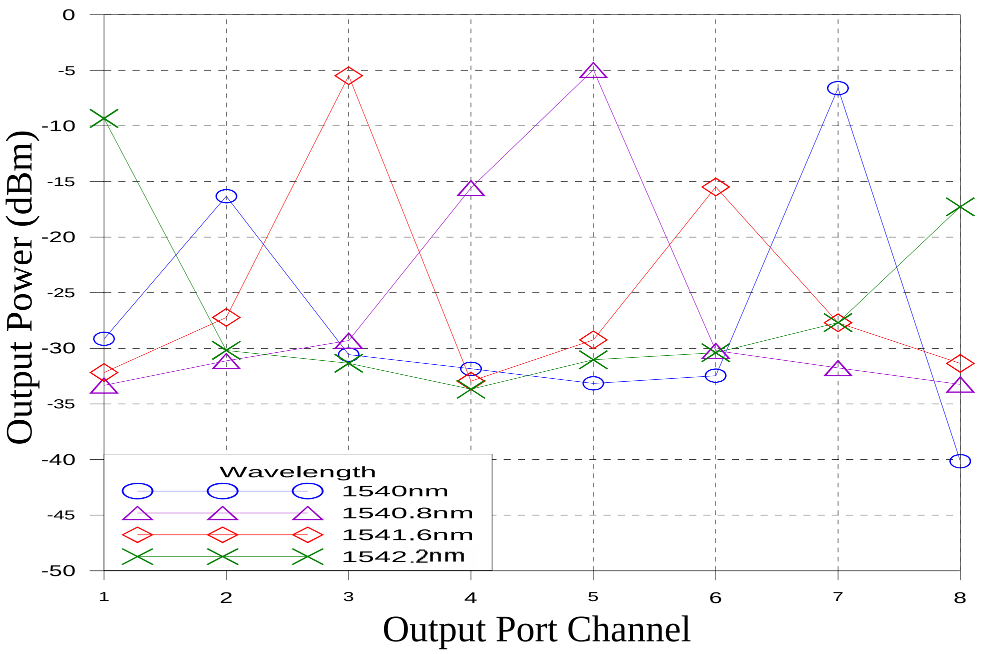

Fig. 3-25 The output power at individual 4 output ports with different refractive index change for ITU wavelength launching into 8×8 grid array microring resonator wavelength switch device

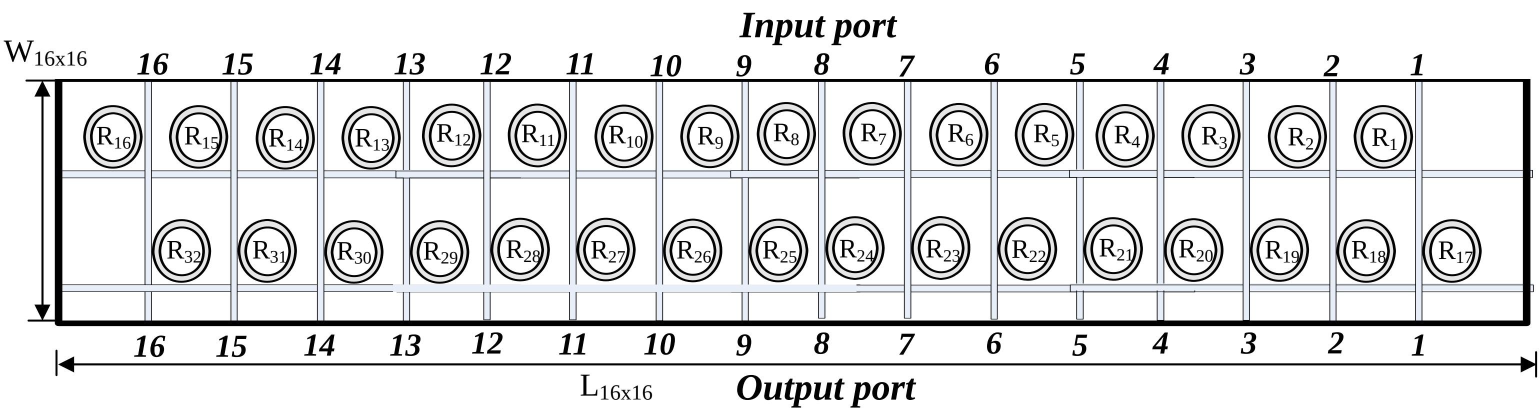

Fig. 3-26 Schematic Diagram of 16×16 Grid Array Microring Resonator Wavelength Switch

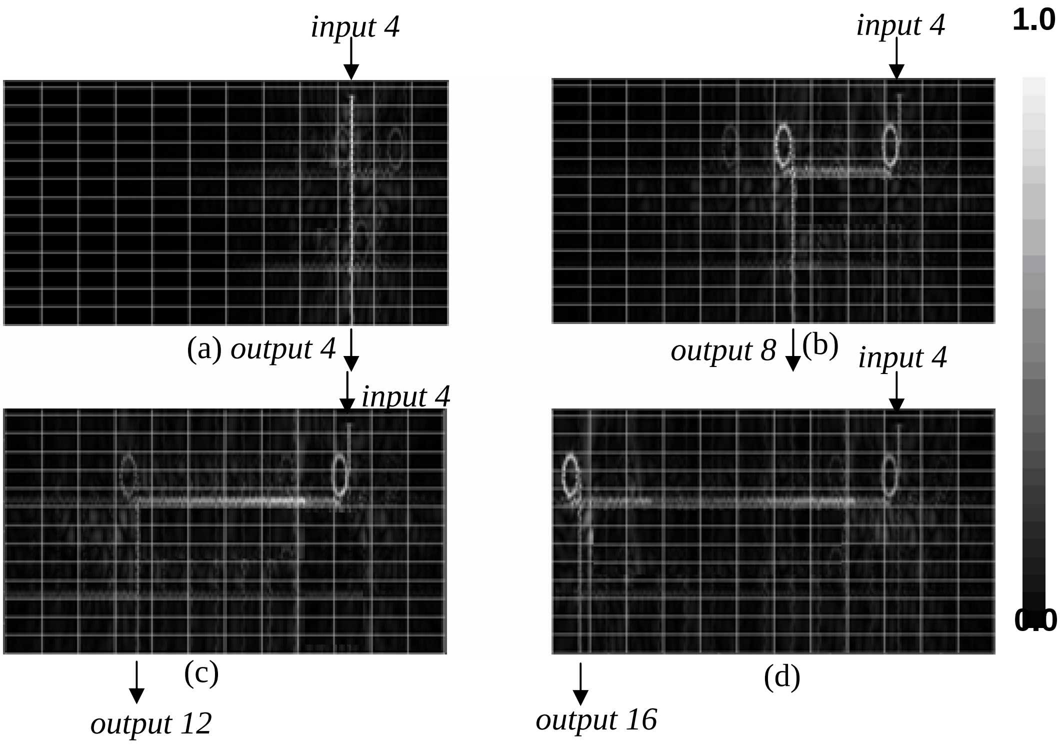

Fig. 3-27 The simulation results of (*a*) output port 4, (*b*) output port 8, (*c*) output port 12, (*d*) output port 16 for the wavelength 1540 nm launching into input port 4 at 16×16 grid array microring resonator wavelength switch with $\mathbf{\Delta}n = -2.4\times10^{-2}$

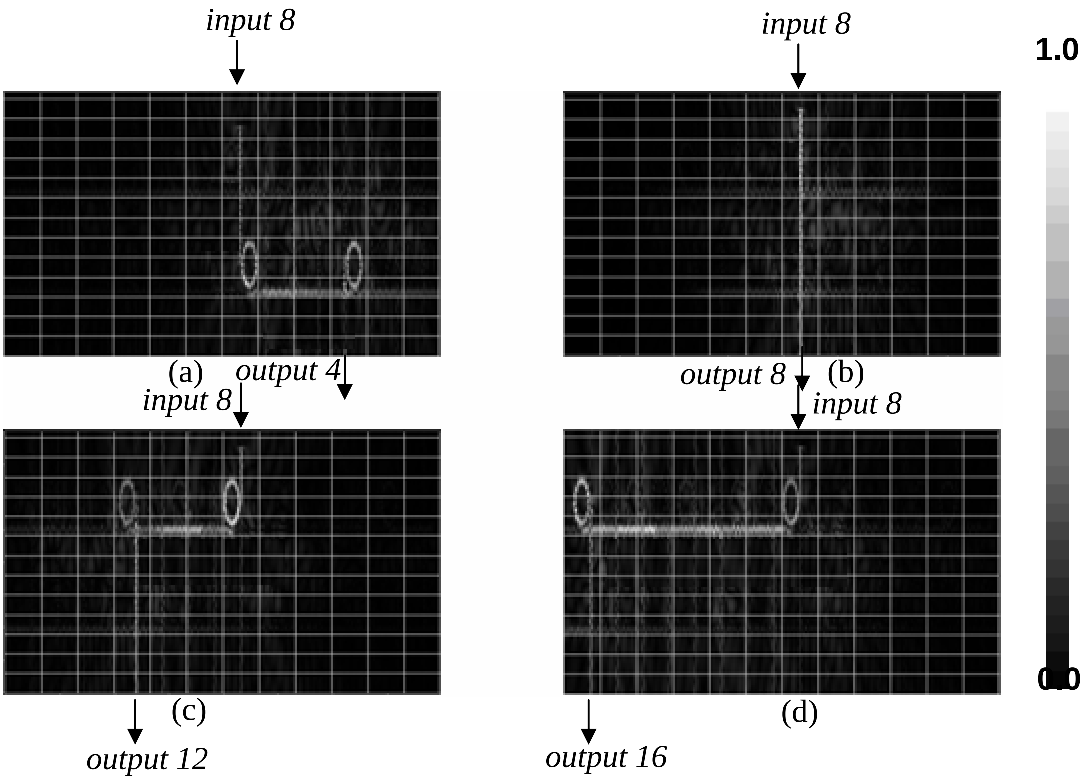

Fig. 3-28 The simulation results of (*a*) output port 4, (*b*) output port 8, (*c*) output port 12, (*d*) output port 16 for the wavelength 1540 nm launching into input port 8 at 16×16 grid array microring resonator wavelength switch with $\mathbf{\Delta}n = -2.4\times10^{-2}$

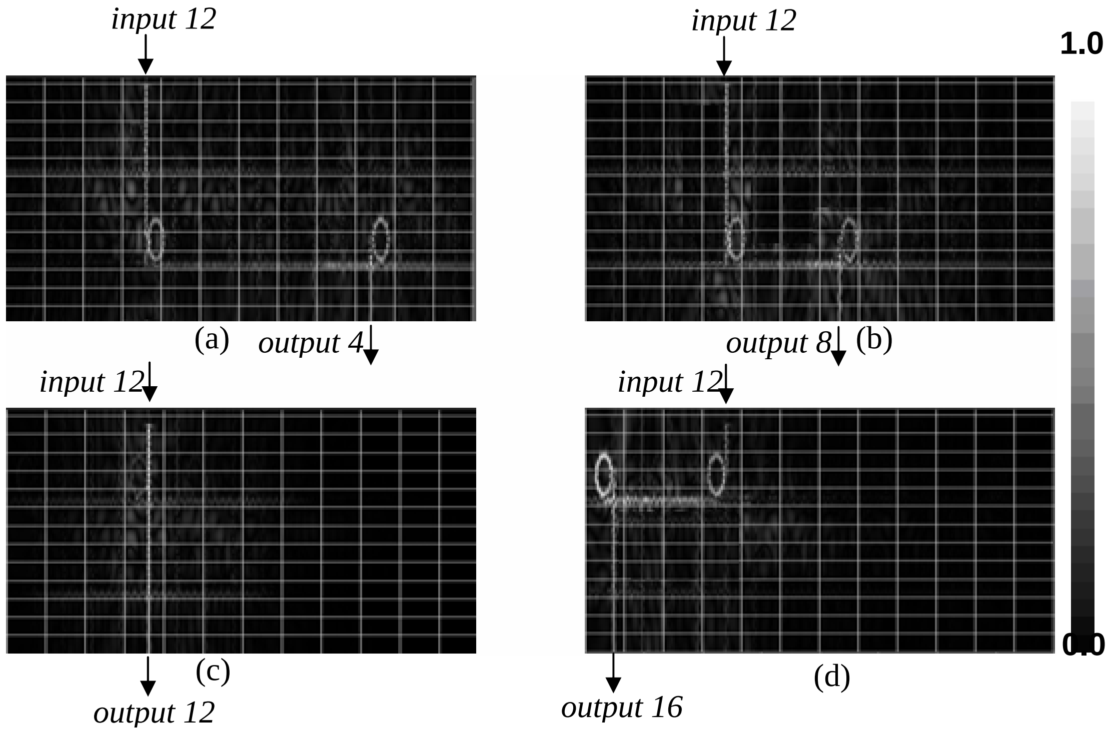

Fig. 3-29 The simulation results of (*a*) output port 4, (*b*) output port 8, (*c*) output port 12, (*d*) output port 16 for the wavelength 1540 nm launching into input port 12 at 16×16 grid array microring resonator wavelength switch with Δn= –2.4×10^{-2}

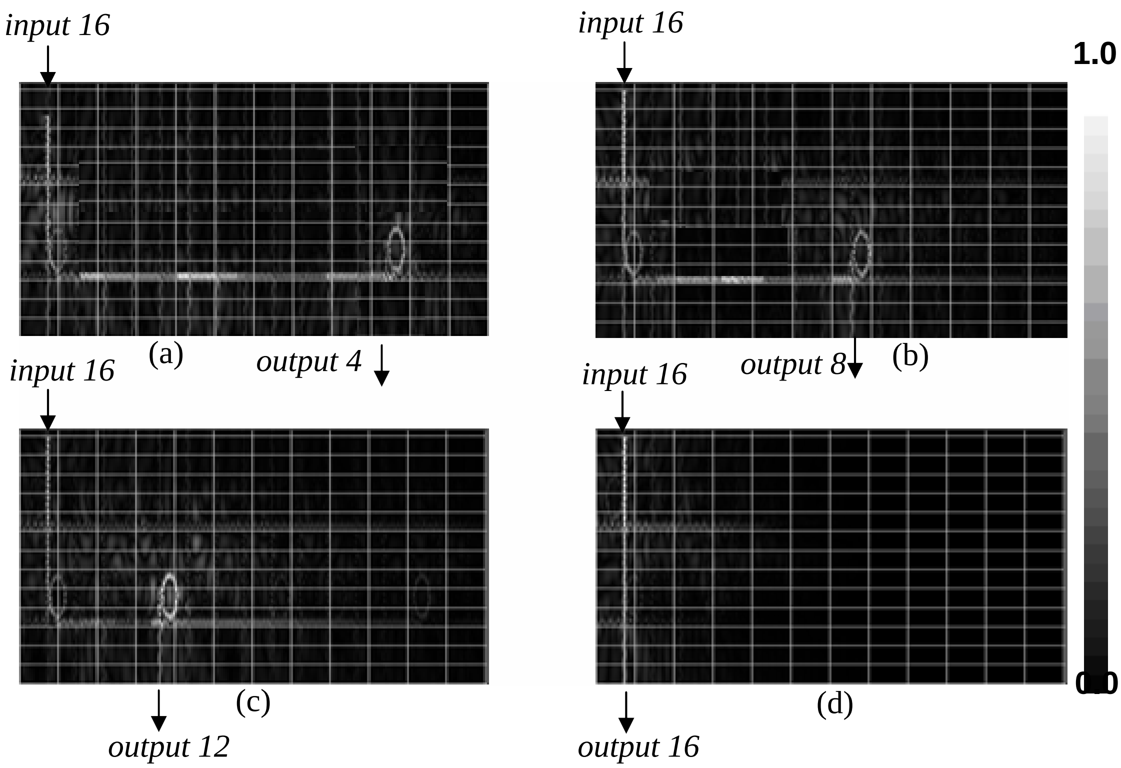

Fig. 3-30 The simulation results of (*a*) output port 4, (*b*) output port 8, (*c*) output port 12, (*d*) output port 16 for the wavelength 1540 nm launching into input port 16 at 16×16 grid array microring resonator wavelength switch with Δn= –2.4×10^{-2}

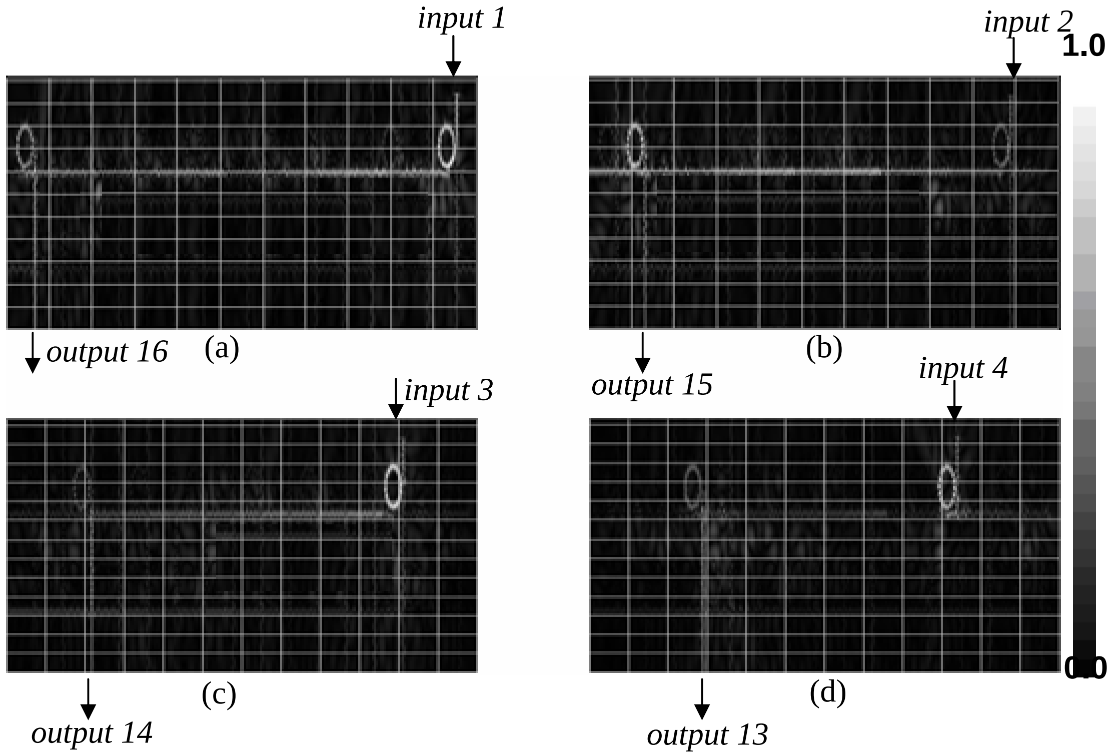

Fig. 3-31 The simulation results of (a)-(d) for ITU wavelength launching into 16×16 grid array microring resonator wavelength switch from input port 1 to input port 4

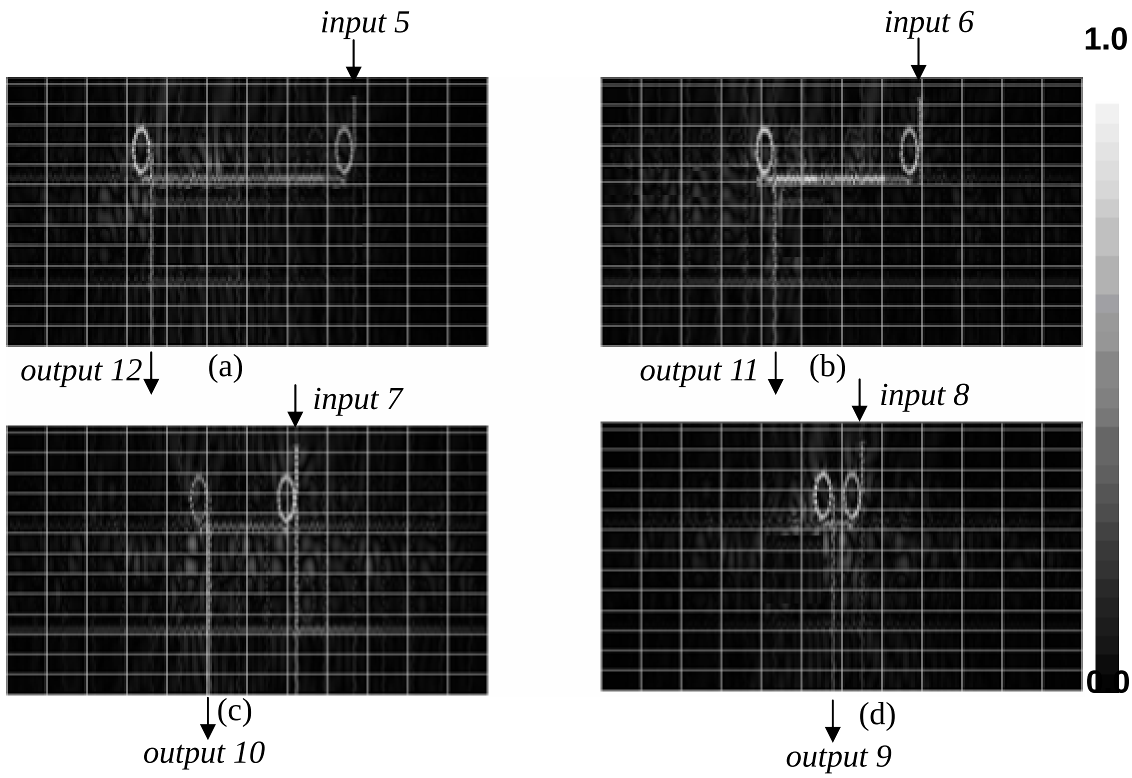

Fig. 3-32 The simulation results of (a)-(d) for ITU wavelength launching into 16×16 grid array microring resonator wavelength switch from input port 5 to input port 8

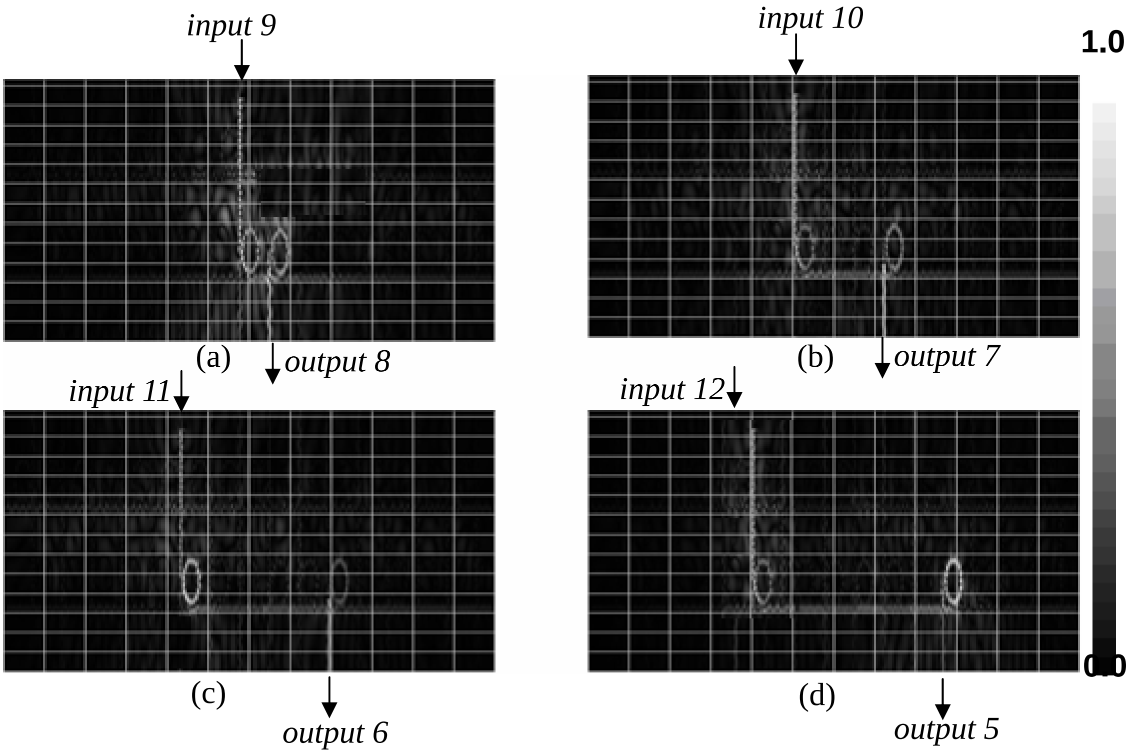

Fig. 3-33 The simulation results of (a)-(d) for ITU wavelength launching into 16×16 grid array microring resonator wavelength switch from input port 9 to input port 12

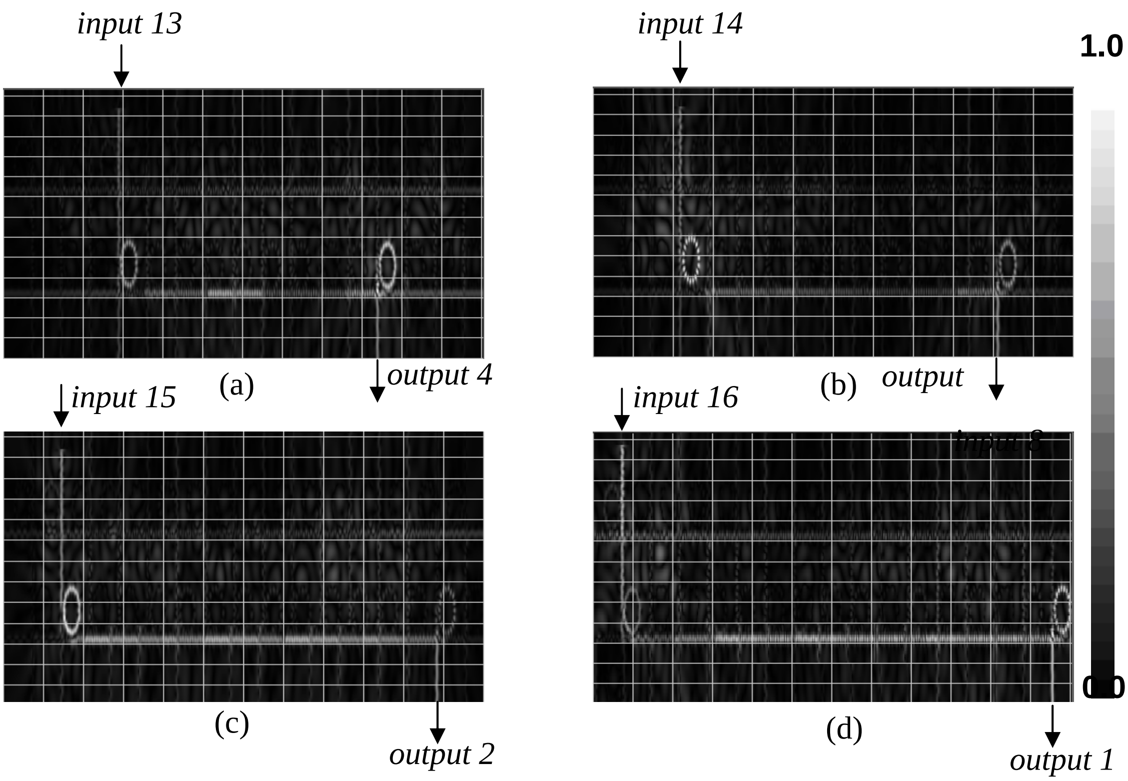

Fig. 3-34 The simulation results of (a)-(d) for ITU wavelength launching into 16×16 grid array microring resonator wavelength switch from input port 13 to input port 16

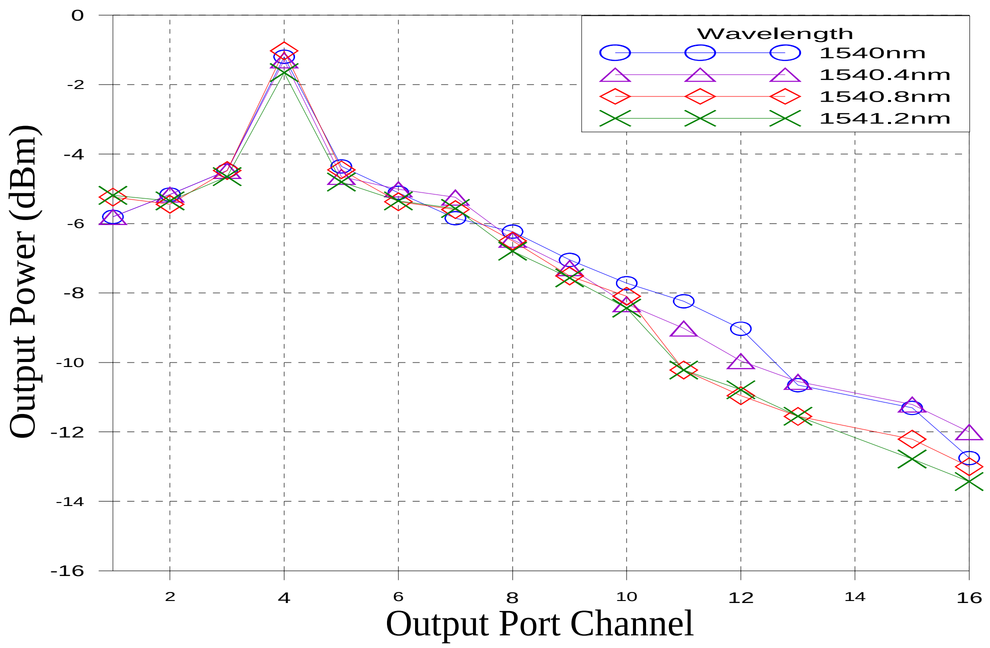

Fig. 3-35 The output power at individual output channel with different refractive index change for the four wavelength individual launching into 16×16 grid array microring resonator wavelength switch input port 4

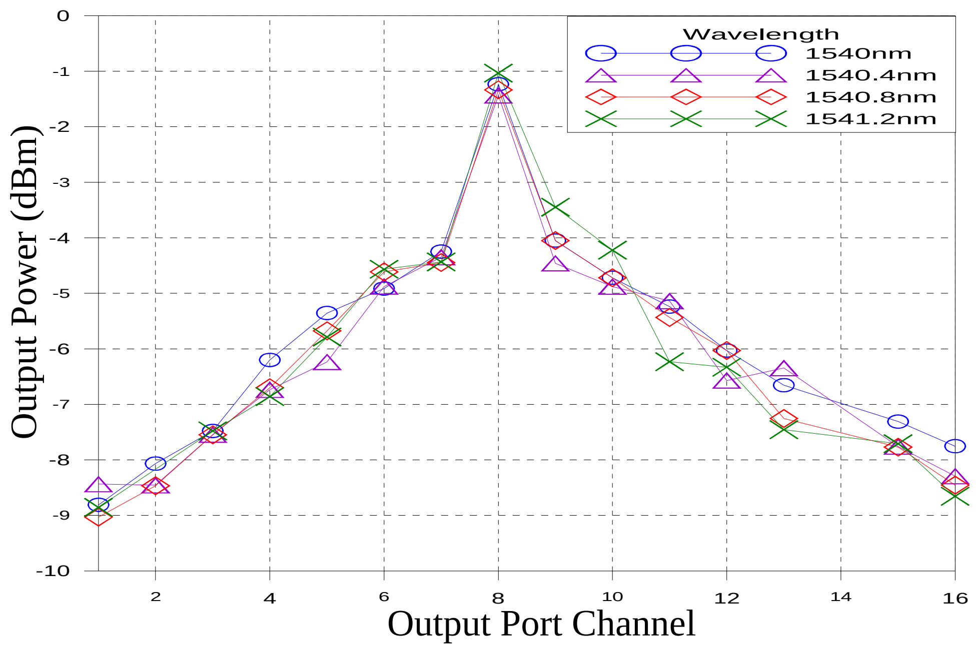

Fig. 3-36 The output power at individual output channel with different refractive index change for the four wavelength individual launching into 16×16 grid array microring resonator wavelength switch input port 8

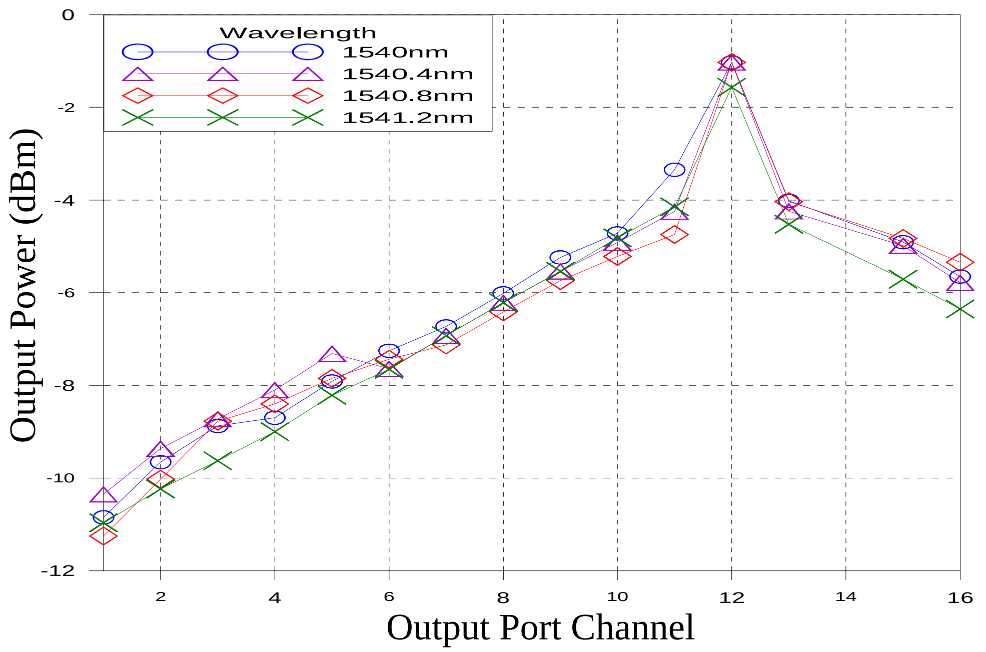

Fig. 3-37 The output power at individual output channel with different refractive index change for the four wavelength individual launching into 16×16 grid array microring resonator wavelength switch input port 12

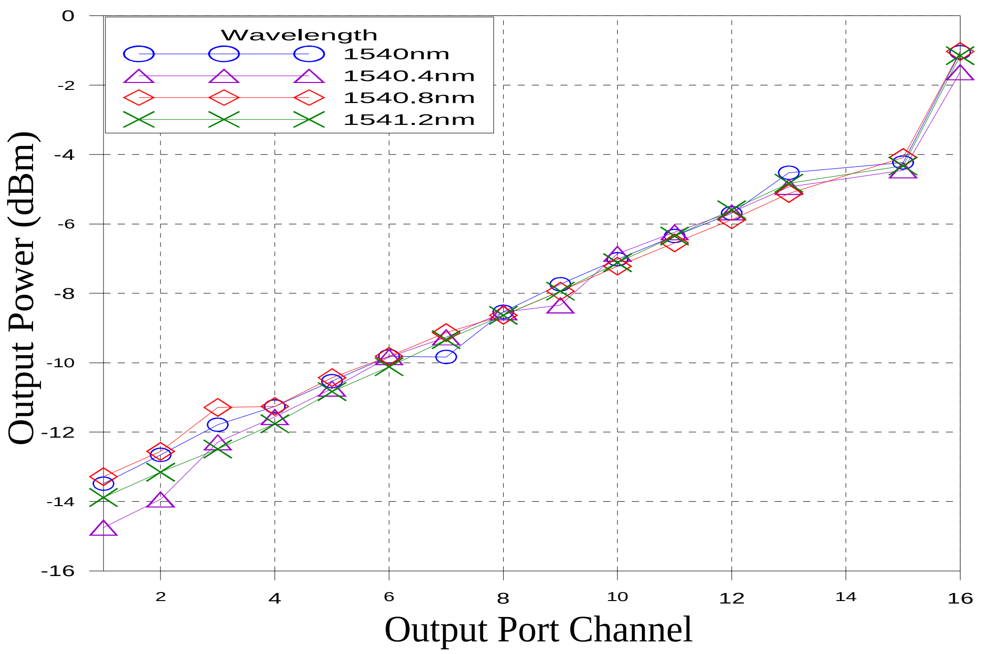

Fig. 3-38 The output power at individual output channel with different refractive index change for the four wavelength individual launching into 16×16 grid array microring resonator wavelength switch input port 16

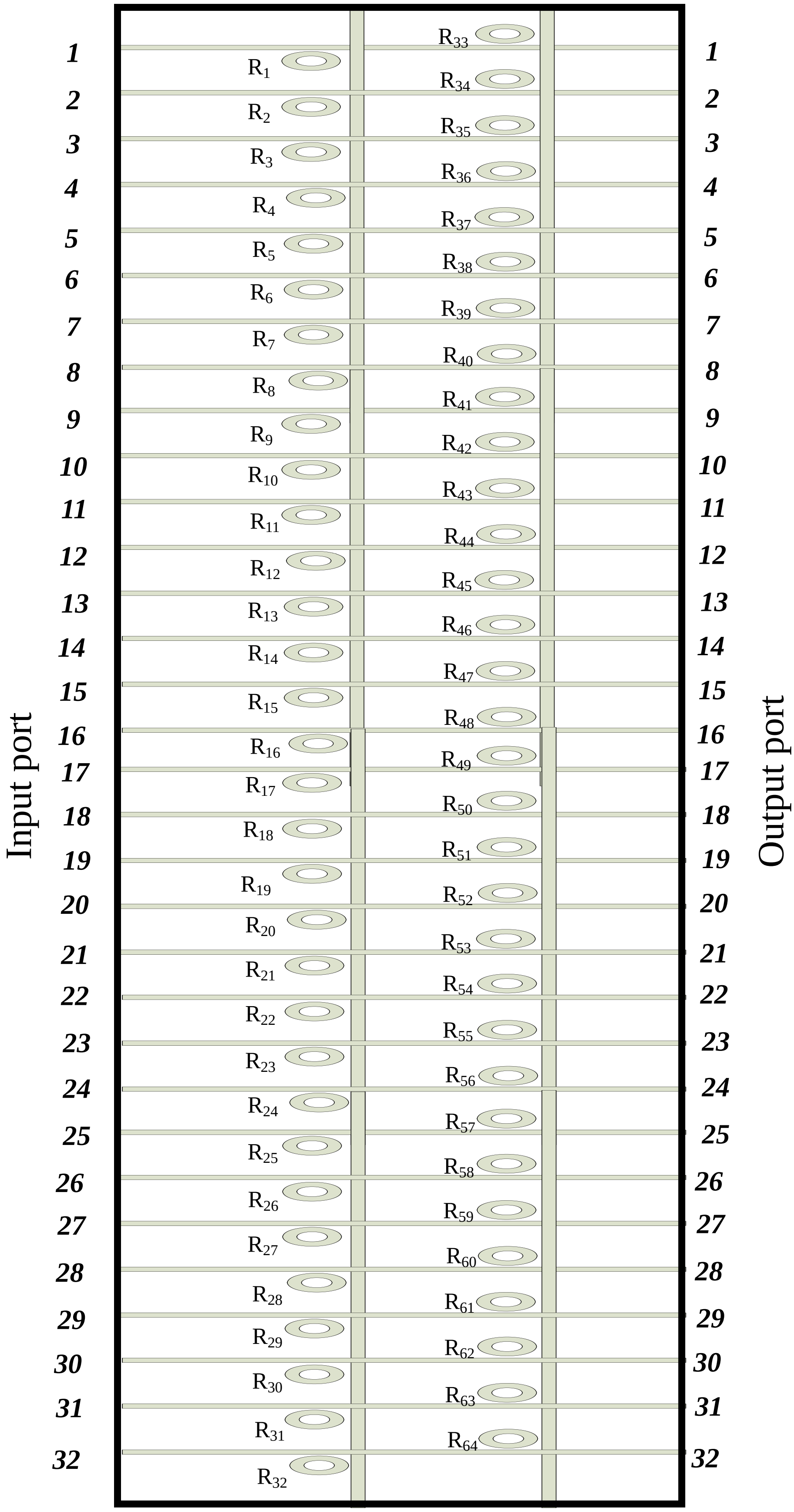

Fig. 3-40 Schematic Diagram of 32×32 Grid Array Microring Resonator Wavelength Switch

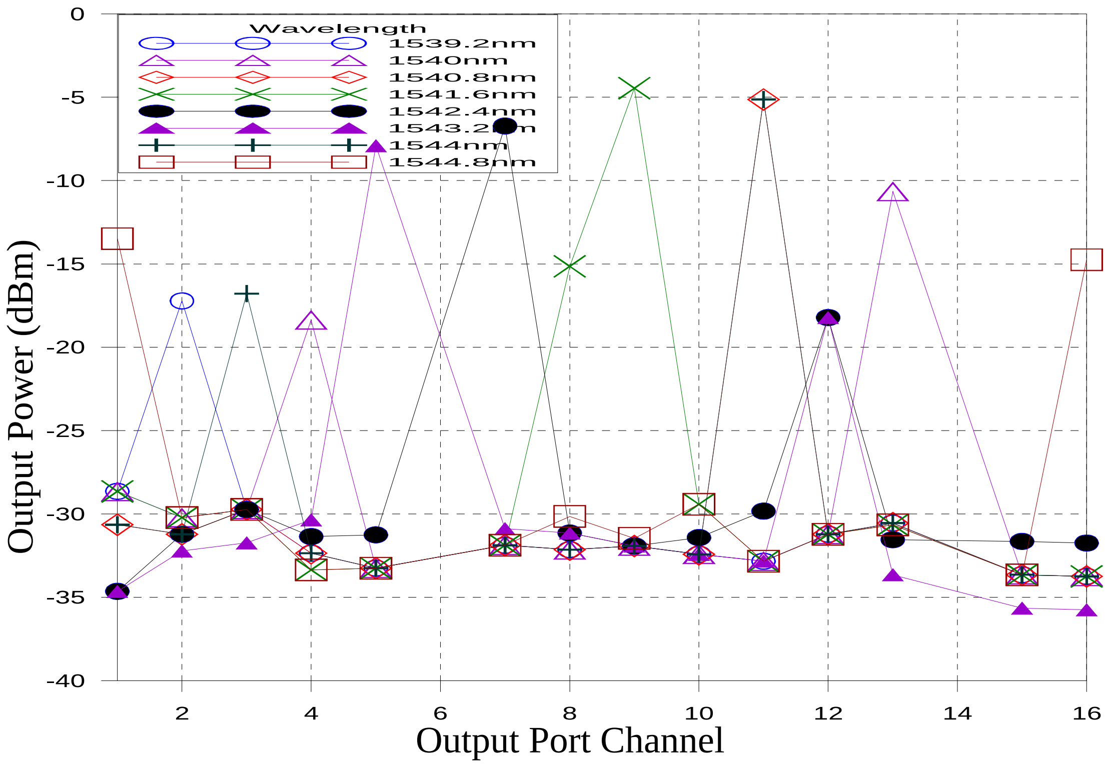

Fig. 3-39 The output power at individual 8 output ports with different refractive index change for ITU wavelength launching into 16×16 grid array microring resonator wavelength switch device

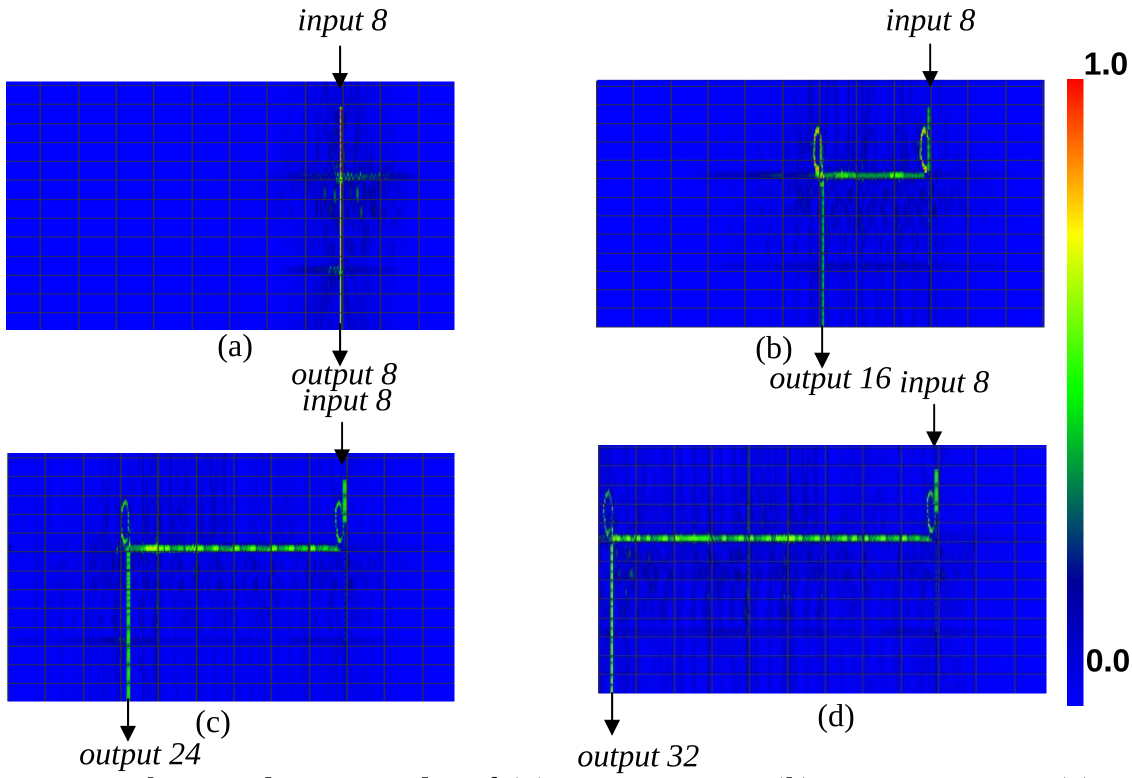

Fig. 3-41 The simulation results of (*a*) output port 8, (*b*) output port 16, (*c*) output port 24, (*d*) output port 32 for the wavelength 1540 nm launching into input port 8 at 32×32 grid array microring resonator wavelength switch with $\Delta n = -2.4\times10^{-2}$

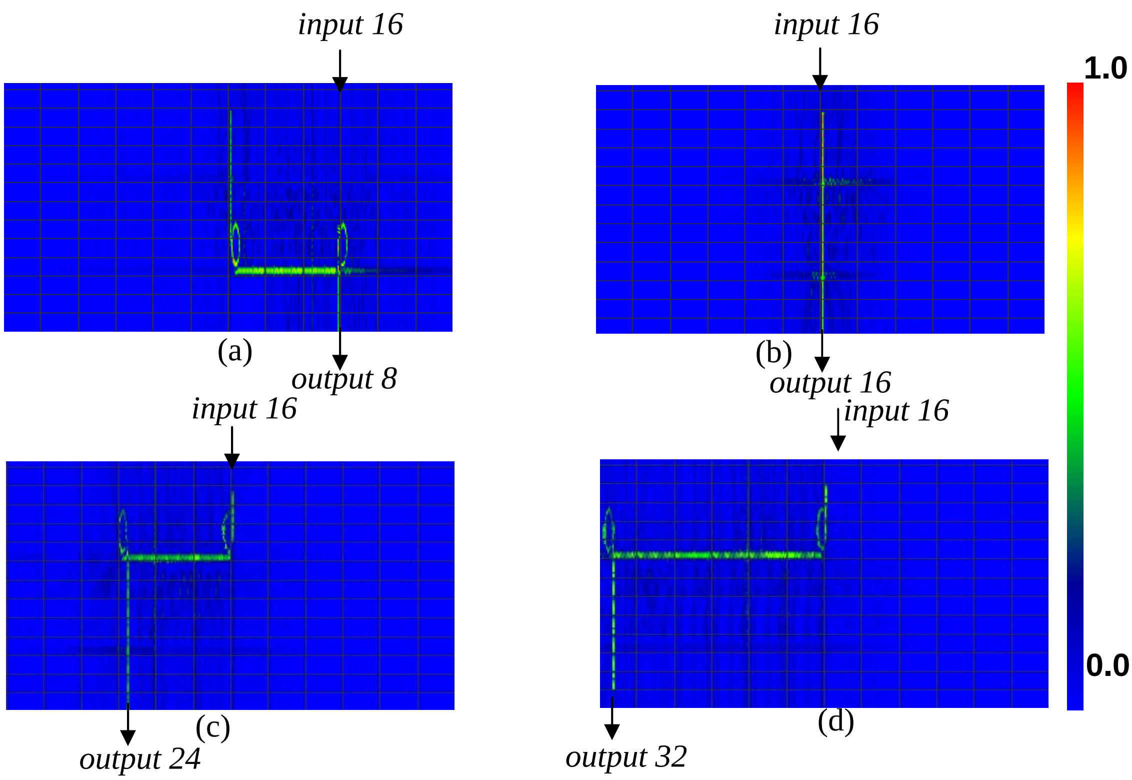

Fig. 3-42 The simulation results of (*a*) output port 8, (*b*) output port 16, (*c*) output port 24, (*d*) output port 32 for the wavelength 1540 nm launching into input port 16 at 32×32 grid array microring resonator wavelength switch with $\Delta n = -2.4\times10^{-2}$

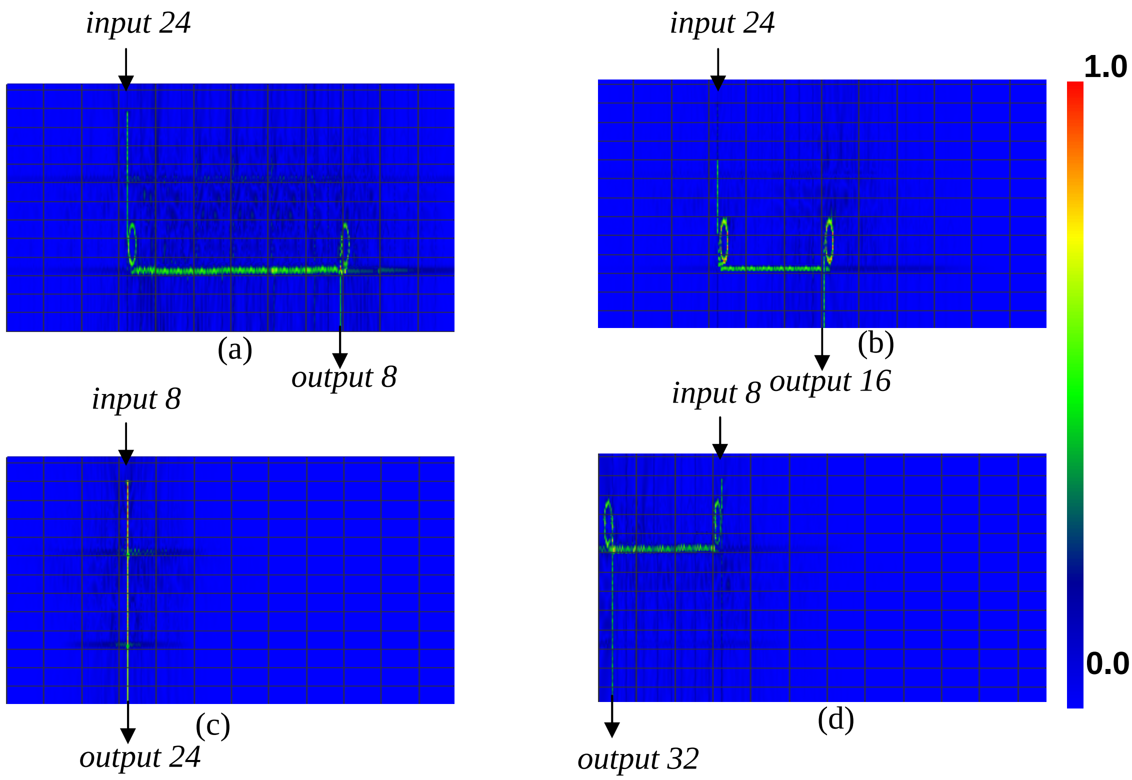

Fig. 3-43 The simulation results of (*a*) output port 8, (*b*) output port 16, (*c*) output port 24, (*d*) output port 32 for the wavelength 1540 nm launching into input port 24 at 32×32 grid array microring resonator wavelength switch with $\Delta n = -2.4\times10^{-2}$

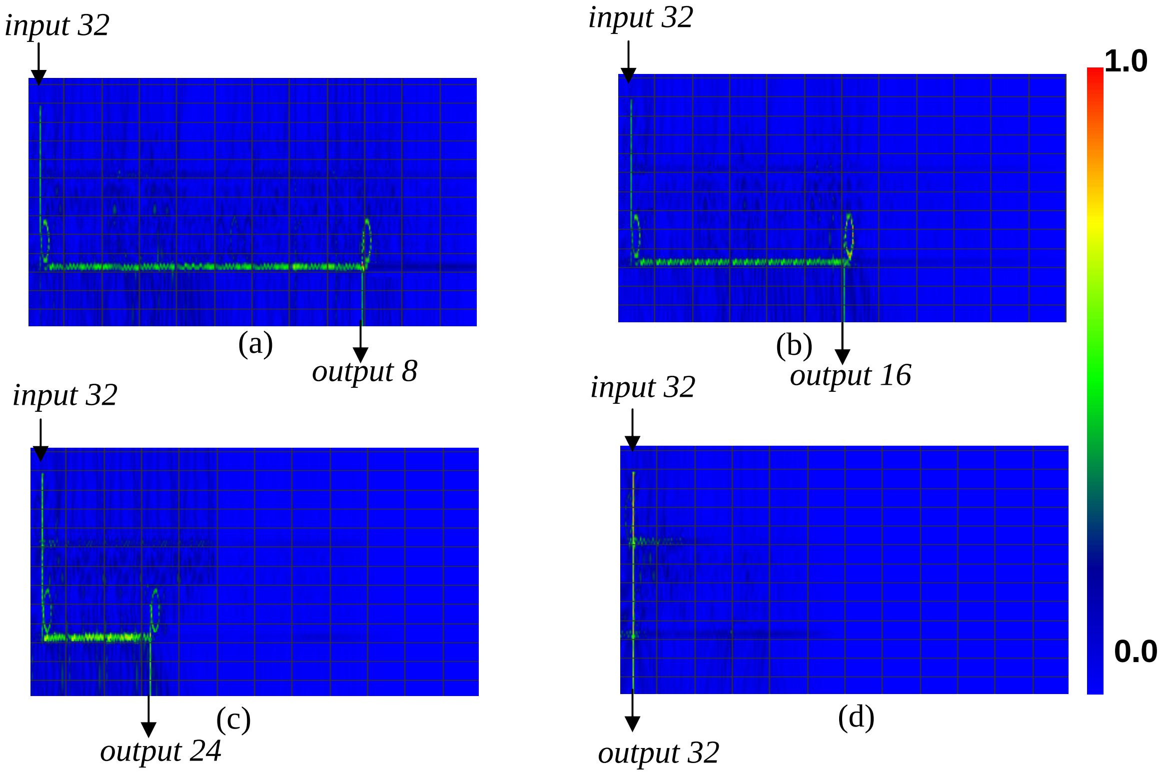

Fig. 3-44 The simulation results of (*a*) output port 8, (*b*) output port 16, (*c*) output port 24, (*d*) output port 32 for the wavelength 1540 nm launching into input port 32 at 32×32 grid array microring resonator wavelength switch with $\Delta n = -2.4\times10^{-2}$

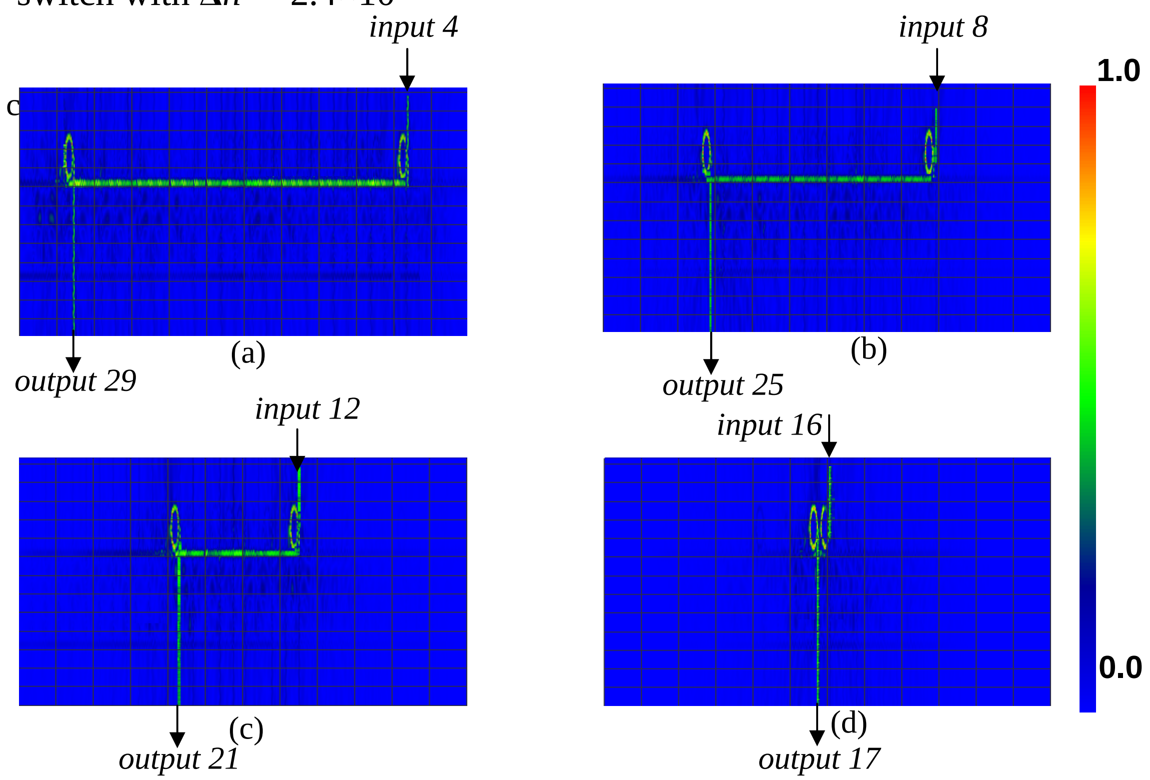

Fig. 3-45 The simulation results of (a)-(d) for ITU wavelength launching into 32×32 grid array microring resonator wavelength switch from input port 4 to input port 16

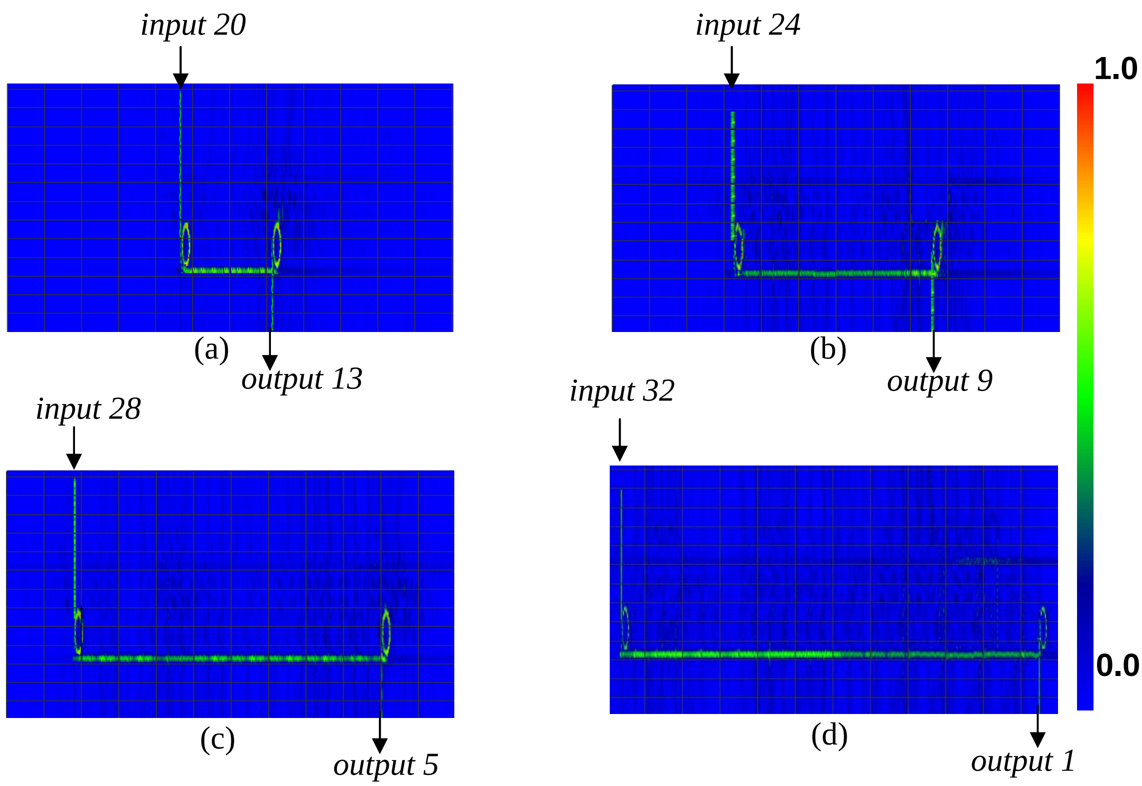

Fig. 3-46 The simulation results of (a)-(d) for ITU wavelength launching into 32×32 grid array microring resonator wavelength switch from input port 20 to input port 32

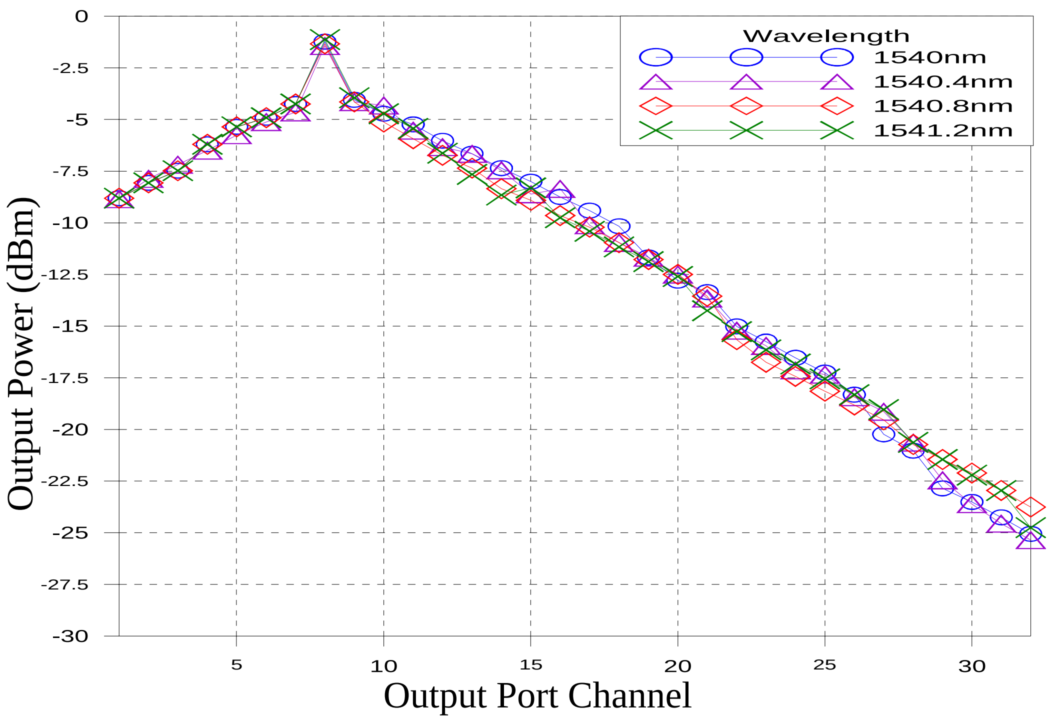

Fig. 3-47 The output power at individual output channel with different refractive index change for the four wavelength individual launching into 32×32 grid array microring resonator wavelength switch input port 8

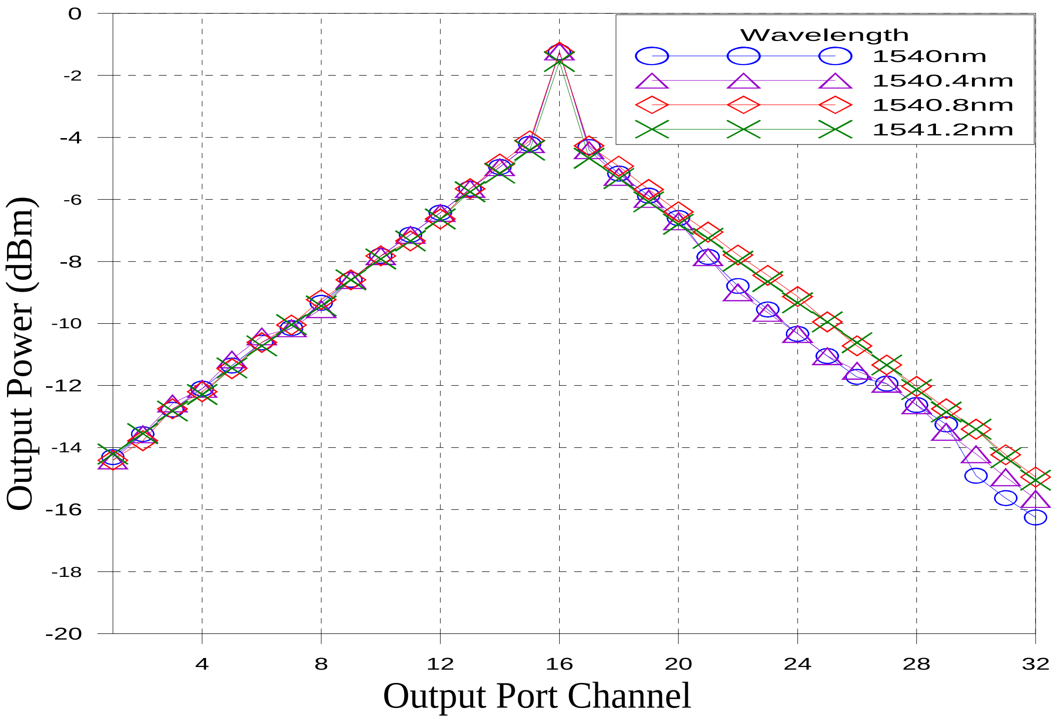

Fig. 3-48 The output power at individual output channel with different refractive index change for the four wavelength individual launching into 32×32 grid array microring resonator wavelength switch input port 16

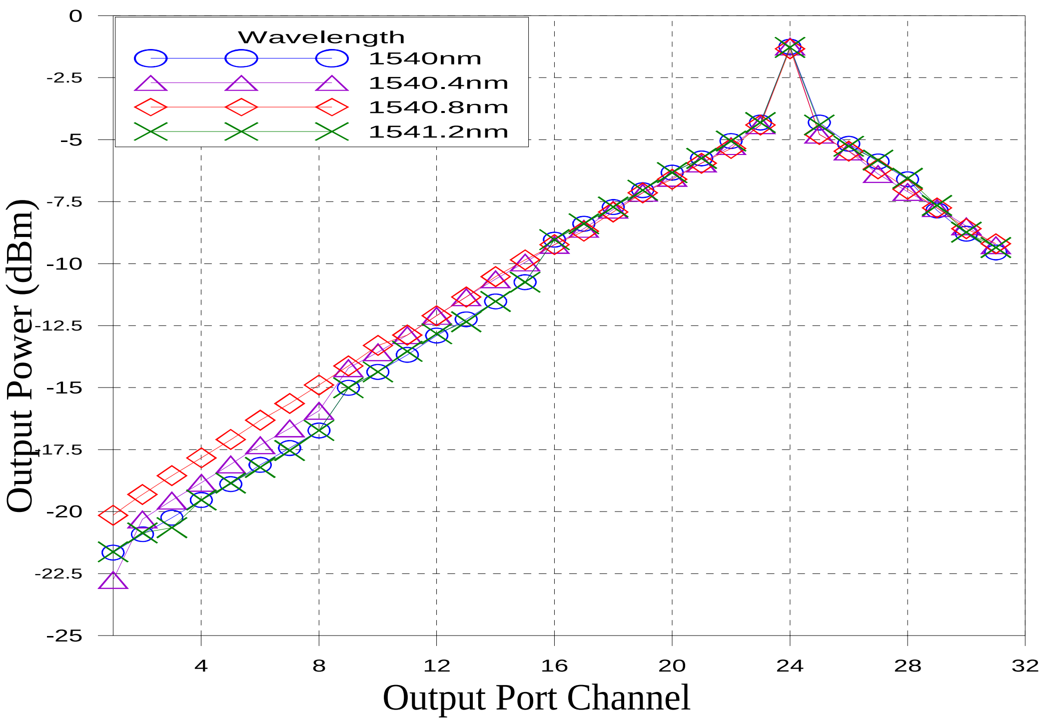

Fig. 3-49 The output power at individual output channel with different refractive index change for the four wavelength individual launching into 32×32 grid array microring resonator wavelength switch input port 24

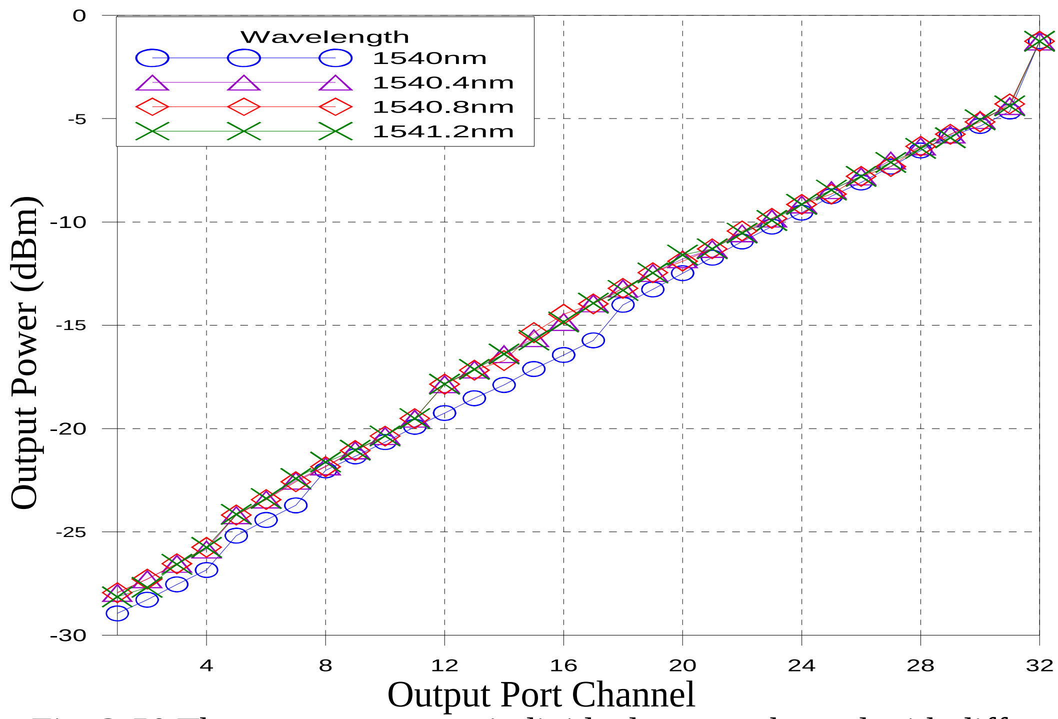

Fig. 3-50 The output power at individual output channel with different refractive index change for the four wavelength individual launching into 32×32 grid array microring resonator wavelength switch input port 32

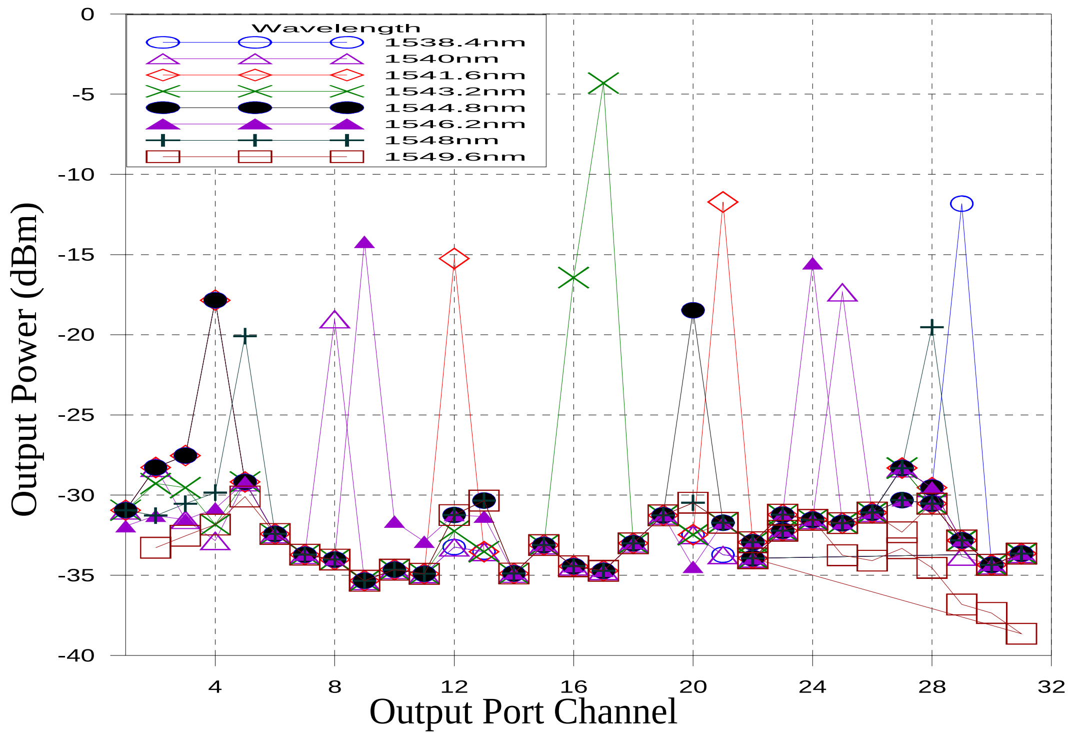

Fig. 3-51 The output power at individual 8 output ports with different refractive index change for ITU wavelength launching into 32×32 grid array microring resonator wavelength switch device

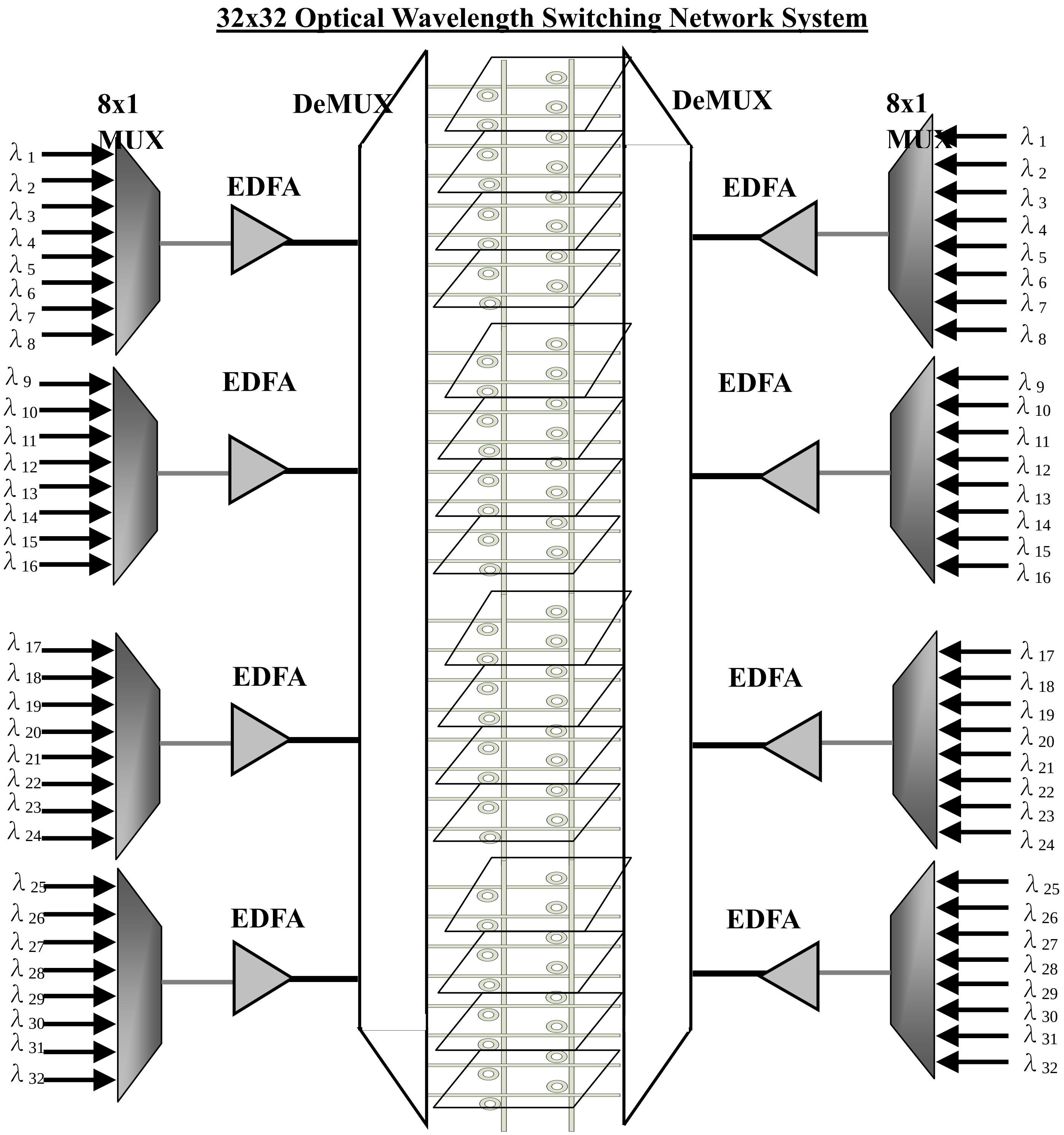

Fig. 3-52 The Bidirectional optical cross-connect schematic diagram of cascade-able 32×32optical wavelength switching with microring

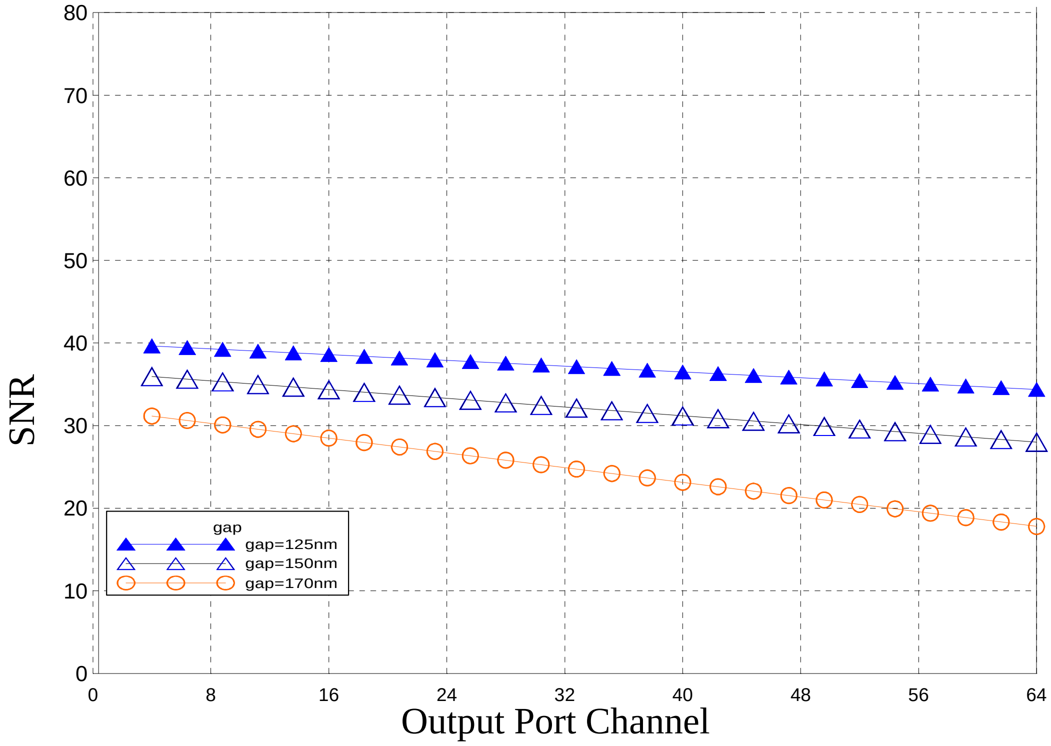

Fig. 3-53 Relation of SNR versus output channel number at different gap